

Twentieth-Century Global-Mean Sea Level Rise: Is the Whole Greater than the Sum of the Parts?

J. M. GREGORY,^a N. J. WHITE,^b J. A. CHURCH,^b M. F. P. BIERKENS,^c J. E. BOX,^d
M. R. VAN DEN BROEKE,^e J. G. COGLEY,^f X. FETTWEIS,^g E. HANNA,^h P. HUYBRECHTS,ⁱ
L. F. KONIKOW,^j P. W. LECLERCQ,^e B. MARZEION,^k J. OERLEMANS,^c M. E. TAMISIEA,^l
Y. WADA,^m L. M. WAKE,ⁿ AND R. S. W. VAN DE WAL^c

^a NCAS-Climate, University of Reading, Reading, and Met Office Hadley Centre, Exeter, United Kingdom

^b CAWCR, CSIRO Marine and Atmospheric Research, Hobart, Australia

^c Department of Physical Geography, Utrecht University, Utrecht, and Deltares, Delft, Netherlands

^d Byrd Polar Research Center, and Department of Geography, Atmospheric Sciences Program,
The Ohio State University, Columbus, Ohio

^e Institute for Marine and Atmospheric Research Utrecht, Utrecht University, Utrecht, Netherlands

^f Department of Geography, Trent University, Peterborough, Ontario, Canada

^g Département de Géographie, Université de Liège, Liège, Belgium, and Institute for Marine and
Atmospheric Research Utrecht, Utrecht University, Utrecht, Netherlands

^h Department of Geography, University of Sheffield, Sheffield, United Kingdom

ⁱ Earth System Sciences, and Departement Geografie, Vrije Universiteit Brussel, Brussels, Belgium

^j U.S. Geological Survey, Reston, Virginia

^k Centre of Climate and Cryosphere, Institute of Meteorology and Geophysics, University of Innsbruck, Innsbruck, Austria

^l National Oceanography Centre, Liverpool, United Kingdom

^m Department of Physical Geography, Utrecht University, Utrecht, Netherlands

ⁿ Department of Geography, University of Calgary, Calgary, Canada

(Manuscript received 1 June 2012, in final form 8 November 2012)

ABSTRACT

Confidence in projections of global-mean sea level rise (GMSLR) depends on an ability to account for GMSLR during the twentieth century. There are contributions from ocean thermal expansion, mass loss from glaciers and ice sheets, groundwater extraction, and reservoir impoundment. Progress has been made toward solving the “enigma” of twentieth-century GMSLR, which is that the observed GMSLR has previously been found to exceed the sum of estimated contributions, especially for the earlier decades. The authors propose the following: thermal expansion simulated by climate models may previously have been underestimated because of their not including volcanic forcing in their control state; the rate of glacier mass loss was larger than previously estimated and was not smaller in the first half than in the second half of the century; the Greenland ice sheet could have made a positive contribution throughout the century; and groundwater depletion and reservoir impoundment, which are of opposite sign, may have been approximately equal in magnitude. It is possible to reconstruct the time series of GMSLR from the quantified contributions, apart from a constant residual term, which is small enough to be explained as a long-term contribution from the Antarctic ice sheet. The reconstructions account for the observation that the rate of GMSLR was not much larger during the last 50 years than during the twentieth century as a whole, despite the increasing anthropogenic forcing. Semiempirical methods for projecting GMSLR depend on the existence of a relationship between global climate change and the rate of GMSLR, but the implication of the authors’ closure of the budget is that such a relationship is weak or absent during the twentieth century.

1. Introduction

Confidence in projections of global-mean sea level rise (GMSLR) for the twenty-first century and beyond depends on an understanding of the contributory effects, verified by a demonstrable ability to account for sea level rise during the twentieth century. The relevant

 Denotes Open Access content.

Corresponding author address: J. M. Gregory, Meteorology Building, University of Reading, P.O. Box 243, Reading RG6 6BB, United Kingdom.
E-mail: j.m.gregory@reading.ac.uk

DOI: 10.1175/JCLI-D-12-00319.1

© 2013 American Meteorological Society

effects on multidecadal time scales are thermal expansion due to heat uptake by the global ocean, mass loss from the Greenland and Antarctic ice sheets, mass loss from glaciers, and changes in water storage on land due principally to groundwater depletion and reservoir construction. Improved observational estimates of all these terms have helped to clarify the budget of GMSLR in recent decades. In the analysis of Church et al. (2011) for 1972–2008, the linear trend in GMSLR from tide gauge data of $1.8 \pm 0.2 \text{ mm yr}^{-1}$ is compared with a linear trend from the sum of the contributions of $1.8 \pm 0.4 \text{ mm yr}^{-1}$, among which thermal expansion and glaciers are the largest.

Considering the twentieth century as a whole, Munk (2002) described GMSLR as an “enigma”: it began too early, it had too linear a trend, and it was too large. The first two problems relate to an expectation, based on a general understanding of the processes concerned, that in a warmer climate the rates of thermal expansion and of glacier mass loss will tend to increase. Therefore, we might suppose that these climate-related contributions to GMSLR increased during the twentieth century. However, the trend of GMSLR during recent decades was actually not very much larger than during the twentieth century as a whole. For instance, Church and White (2011) find $1.9 \pm 0.4 \text{ mm yr}^{-1}$ for 1961–2009 and $1.7 \pm 0.2 \text{ mm yr}^{-1}$ for 1900–2009. The third problem, of GMSLR being too large, is shown by the model-derived estimates of contributions reported by Church et al. (2001), which could explain only 50% of twentieth-century GMSLR; likewise, Moore et al. (2011) identify a substantial residual for 1850–1950.

To balance the budget and explain the form of the time series requires time-dependent information about the contributions to GMSLR throughout the century. We are enabled to make progress by new work summarized in this paper regarding the contributions from thermal expansion, glaciers, the Greenland ice sheet, groundwater depletion, and reservoir impoundment, which we address in turn in sections 2–5. Significant uncertainty remains regarding the twentieth-century contribution from the Antarctic ice sheet, for which there are no observational time series or models based on observational input. Some of the time series we use for contributions have stated uncertainties, but instead of using these we have regarded the spread of different estimates for a given quantity as an informal indication of systematic uncertainty. This is partly for simplicity, since the analysis is already complicated by the number of datasets involved, and partly because the uncertainties stated in some cases do not reflect all possible sources of systematic error. We do not have space in this

paper to examine in detail the assumptions involved and the basis of the uncertainty estimates for all the datasets.

In section 6 we compare several recent observational time series of GMSLR, and in section 7 we examine whether these can be accounted for by various combinations of the contributions. This approach has an analogous aim to but differs from the detection and attribution of climate change (e.g., Stott et al. 2010). Studies of that kind seek to attribute the observed changes in the climate system to the agents that forced those changes to occur (e.g., anthropogenic greenhouse gases and tropospheric aerosols, volcanic stratospheric aerosol, and changes in solar irradiance), whereas we attempt to attribute the observed GMSLR to changes in the climate system (in the ocean, land-ice, and land-water storage). Our approach also differs from that of Mitrovica et al. (2001) and subsequent authors, who have compared the spatial pattern of observed sea level change with the patterns expected for different contributions in order to apportion the global mean among those contributions. That method uses spatial information about sea level but not temporal information, whereas we use temporal information but not spatial information.

Before going further, we would like to clarify our terminology. By “thermal expansion,” we mean the contribution to GMSLR from change in seawater density due to change in temperature. We propose a new word “barystatic” for the contribution to GMSLR from the change in the mass of the ocean. A new term would be helpful because the word “eustatic” is now used with various different meanings and has consequently become confusing. The barystatic effect on sea level change is the mass of freshwater added or removed, converted to a volume using a reference density of 1000 kg m^{-3} , and divided by the ocean surface area. It does not include the effects on regional sea level associated with changes in the gravity field and the solid earth (discussed in section 7d) or in salinity. Although salinity change is important to regional sea level change, in the global mean the halosteric effect of adding freshwater to the ocean is practically zero (Munk 2003; Lowe and Gregory 2006, appendix A).

2. Thermal expansion

The contribution to GMSLR due to thermal expansion is calculated from the change in ocean interior temperatures as $-1/A \int \Delta\rho/\rho_0 dV$, where A is the ocean surface area, $\Delta\rho$ is the change in in situ density due to temperature change, ρ_0 is a reference density, and the integral is over ocean volume. Ocean observations

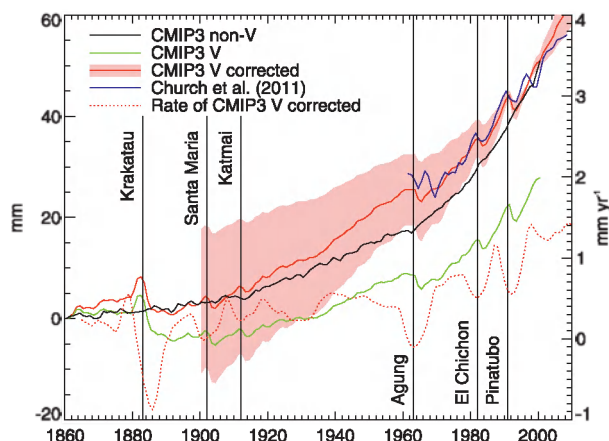


FIG. 1. Time series of the contribution of thermal expansion to global-mean sea level rise. Solid lines and left-hand axis (mm): contribution to global-mean sea level relative to zero in 1860 according to the ensemble means of CMIP3 V and non-V models (i.e., with and without volcanic forcing, respectively), of V models adjusted to have the same time-mean rate of rise as non-V models in order to correct for the spinup effect of time-mean volcanic forcing (as explained in section 2), and of the observational estimate for thermal expansion by Church et al. (2011) (vertically positioned to have the same time mean for 1986–2005 as the ensemble mean of corrected V models). The red shaded area is the 5%–95% range of the ensemble of corrected V models. Dotted line and right-hand axis (mm yr^{-1}): contribution to the rate of global-mean sea level rise according to the ensemble mean of CMIP3 V models after the correction, calculated as a trend in overlapping 10-yr periods. The vertical lines indicate the years in which major volcanic eruptions occurred. The negative excursion in the rate of rise begins before the year of each volcanic eruption because the rate is plotted at the center of the 10-yr period from which it is calculated.

before about 1960 are too sparse to allow a useful estimate of the global ocean integral; therefore, we rely on models to make an estimate for the whole twentieth century.

There is a large difference in thermal expansion between models with anthropogenic forcing only (greenhouse gases and aerosols) and those that also include natural forcing (volcanic aerosol and variability in solar irradiance). Volcanic aerosol reflects sunlight and tends to cool the climate. In the atmosphere–ocean general circulation models (AOGCMs) of phase 3 of the Coupled Model Intercomparison Project (CMIP3; http://www-pcmdi.llnl.gov/ipcc/about_ipcc.php), GMSLR due to thermal expansion from 1860 to 2000 is 50 mm for the ensemble mean of the seven without natural forcing (referred to as the “non-V” models; black line in Fig. 1), but only half as large, at 27 mm, for the ensemble mean of the nine with natural forcing (“V” models; green line in Fig. 1). [The non-V models are CGCM3.1(T47), CNRM-CM3, CSIRO Mk3.0, ECHAM5/MPI-OM, GISS-AOM, INM-CM3.0,

TABLE 1. Expanded names of the non-V and V models.

Model	Expansion
Non-V models	
CGCM3.1(T47)	Canadian Centre for Climate Modelling and Analysis (CCCma) Coupled General Circulation Model version 3.1
CNRM-CM3	Centre National de Recherches Météorologiques Coupled Global Climate Model version 3
CSIRO Mk3.0	Commonwealth Scientific and Industrial Research Organisation Mark version 3.0
ECHAM5/MPI-OM	ECHAM5/Max Planck Institute Ocean Model
GISS-AOM	Goddard Institute for Space Studies Atmosphere–Ocean Model
INM-CM3.0	Institute of Numerical Mathematics Coupled Model version 3.0
HadCM3	Third climate configuration of the Met Office Unified Model
V models	
CCSM3	National Center for Atmospheric Research Community Climate System Model, version 3
ECHO-G	ECHAM and the global Hamburg Ocean Primitive Equation
GFDL CM2.0	Geophysical Fluid Dynamics Laboratory Climate Model version 2.0
GFDL CM2.1	Geophysical Fluid Dynamics Laboratory Climate Model version 2.1
GISS-EH	Goddard Institute for Space Studies Model E-H
GISS-ER	Goddard Institute for Space Studies Model E-R
MIROC3.2(medres)	Model for Interdisciplinary Research on Climate 3.2, medium-resolution version
MRI CGCM2.3.2	Meteorological Research Institute Coupled General Circulation Model version 2.3.2
PCM	National Center for Atmospheric Research Parallel Climate Model

and HadCM3. The V models are CCSM3, ECHO-G, GFDL CM2.0, GFDL CM2.1, GISS-EH, GISS-ER, MIROC3.2(medres), MRI CGCM2.3.2, and PCM. See Table 1 for model names.]

Rapid negative excursions in thermal expansion due to cooling of the ocean are evident in the V models following large volcanic eruptions, and it has been proposed that the smaller time-mean thermal expansion in the V models over the twentieth century could be due to a long persistence of the influence of eruptions in the

late nineteenth century, especially Krakatau (Delworth et al. 2005; Gleckler et al. 2006a,b). Alternatively, Gregory (2010) and Gregory et al. (2013) suggested that the difference is an artifact of the experimental design of CMIP3. Because the models have been spun up without volcanic forcing, its imposition during the “historical” simulation (i.e., the experiment starting in the late nineteenth century) gives a time-mean negative forcing and a spurious cooling trend. In reality episodic volcanic eruptions are a normal part of the climate system; therefore its long-term mean state includes their influence.

As an illustration of this idea, let us consider another forcing agent. Methane is also a natural component of atmospheric composition. If an AOGCM were spun up to obtain a control steady state without atmospheric methane and then the nonzero time-dependent historical methane concentration were imposed in a simulation that began from the control state, it is obvious that a spurious warming tendency would be present throughout the historical simulation while the climate system adjusted to the sudden introduction of positive radiative forcing due to methane.

According to this argument, if the V models were run with volcanic forcing through previous millennia, so that by the late nineteenth century they had adjusted to its time-mean influence, they would then give the same model-mean time-mean thermal expansion during the CMIP3 historical simulation (from 1860 to 2000) as the non-V models, provided the following: first, there is no systematic difference between the two groups of AOGCMs in thermal expansion caused by a given radiative forcing; second, the frequency and magnitude of volcanic eruptions in the period of the historical simulations is typical of the preceding centuries. Regarding the first proviso, we find that the model-mean GMSLR due to thermal expansion during the twenty-first century is statistically indistinguishable between the two groups of models (0.24 ± 0.02 m for non-V models; 0.21 ± 0.02 m for V models), under the A1B scenario of the Special Report on Emissions Scenarios used in CMIP3 for projections. The second proviso cannot be verified with the model results from CMIP3 and requires further investigation. However, it is more realistic to assume that 1860–2000 is typical of the long term with respect to volcanic activity than to assume that there are typically no volcanic eruptions, with the latter being the assumption implicit in the CMIP3 design.

Following this argument, in order to correct approximately for the spurious cooling, we add a constant 0.16 mm yr^{-1} to the ensemble-mean time series of historical thermal expansion from V models. This constant is the difference between the V and non-V models in the time-mean rate of thermal expansion for 1860–2000

(thus the red solid line of corrected V models in Fig. 1 meets the black line of the non-V models at 2000). Solar forcing, also included in the V models, is estimated to have increased over this period (Forster et al. 2007), which will have reduced the size of the correction. Making the correction constant in time is a further approximation. In reality the cooling tendency will diminish with time, as the ocean adjusts to the time-mean negative volcanic forcing (Gregory 2010), but the time profile of the adjustment is unknown and very likely to be model dependent.

As a consequence of the correction, we estimate a greater rate of thermal expansion in the early part of the twentieth century than indicated by the CMIP3 historical simulations, because there were no large volcanic eruptions during these decades, so in effect the radiative forcing was positive with respect to the long-term mean (Gregory 2010). There is a clear increase in the corrected V ensemble-mean rate of thermal expansion after 1960 (dotted red line in Fig. 1), consistent with increasing positive anthropogenic forcing and global warming (e.g., Church et al. 2011). During these decades, negative volcanic forcing had a short-term negative effect on the rate of ocean heat uptake, and consequently the non-V ensemble-mean rate of thermal expansion is even larger than the corrected V ensemble mean (cf. the black and red solid lines). Because natural volcanic forcing was weak in the first half of the century and stronger in the second half, it tended to make the rate of thermal expansion more constant during the century than it would have been with anthropogenic forcing alone (cf. Gregory et al. 2006); if our adjustment included a time dependence, it would reinforce this tendency, by increasing the estimated rate of thermal expansion early in the record and reducing it later.

Historical simulations with CMIP3 AOGCMs mostly end in 2000. We append the mean thermal expansion time series from 2000 to 2010 of non-V models under the A1B emissions scenario (no spinup correction is necessary for non-V models). Because the zero of global-mean sea level is arbitrary, we can freely adjust either time series with a constant vertical offset to make them join at 2000, and they match well at 2000 regarding rate of rise. At the time of writing, results are becoming available from CMIP5 AOGCMs, which extend to 2005. We have not used these because they will require detailed analysis, such as the CMIP3 models have received over the last few years, and information is not yet available about whether volcanic forcing was included in the CMIP5 spinup integrations.

Domingues et al. (2008) compared thermal expansion for the upper 700 m for 1961–2003 from CMIP3

AOGCMs with an observational estimate including recent corrections for instrumental biases. They noted that the mean trend of the non-V models is greater than observed, and the mean of the V models is closer to but slightly less than observed. We would not expect the volcanic spinup to cause a large discrepancy in the upper ocean, because the long-term adjustment takes place mainly in the deeper layers.

In the ensemble-mean CMIP3 corrected and extended time series, the rate of thermal expansion is 0.87 mm yr^{-1} for 1972–2008, which is consistent with the observational estimate of $0.80 \pm 0.15 \text{ mm yr}^{-1}$ for the full ocean depth by Church et al. (2011) (both rates are from linear regression against time). There is a remarkably good agreement in time profile between the observational and model estimates (blue and red solid lines in Fig. 1); in particular, both show dips following Agung, El Chichón, and Pinatubo.

The ratio of the ensemble standard deviation to the ensemble mean of GMSLR due to thermal expansion during the twentieth century in corrected CMIP3 V models is about 20%, and the standard error given by Church et al. (2011) for thermal expansion during 1972–2008 is a similar fraction of their central estimate. On this basis, we assume that 20% is a reasonable estimate of the fractional uncertainty in the thermal expansion contribution. Assuming further that the error distribution is normal, we calculate time series for the 5th, 50th, and 95th percentiles (red line and shading in Fig. 1), which we refer to as expansion L for “low,” expansion M for “mid,” and expansion H for “high.” We regard these as alternative possibilities for the budget of sea level change. Time series expansion L has an expansion of 31 mm during the twentieth century, which is close to the ensemble mean of CMIP3 V models without correction (in Fig. 1, the upper limit of the red envelope, which indicates the time profile of least expansion, is roughly parallel to the green line).

3. Glaciers

Records of glacier length from all regions of the world show retreat during the last century (e.g., Fig. 2 of Leclercq et al. 2011), indicating net mass loss, which is consistent with a warming climate worldwide (Oerlemans 2005; Leclercq and Oerlemans 2012). Increased melting can be outweighed by increased snowfall, as in Scandinavia from the mid-1970s to the mid-1990s (Andreassen et al. 2005; Chinn et al. 2005; Kaser et al. 2006; Imhof et al. 2011) and probably in the Karakoram since the late 1990s or earlier (Hewitt 2011; Gardelle et al. 2012), but such episodes of mass gain are short lived and localized.

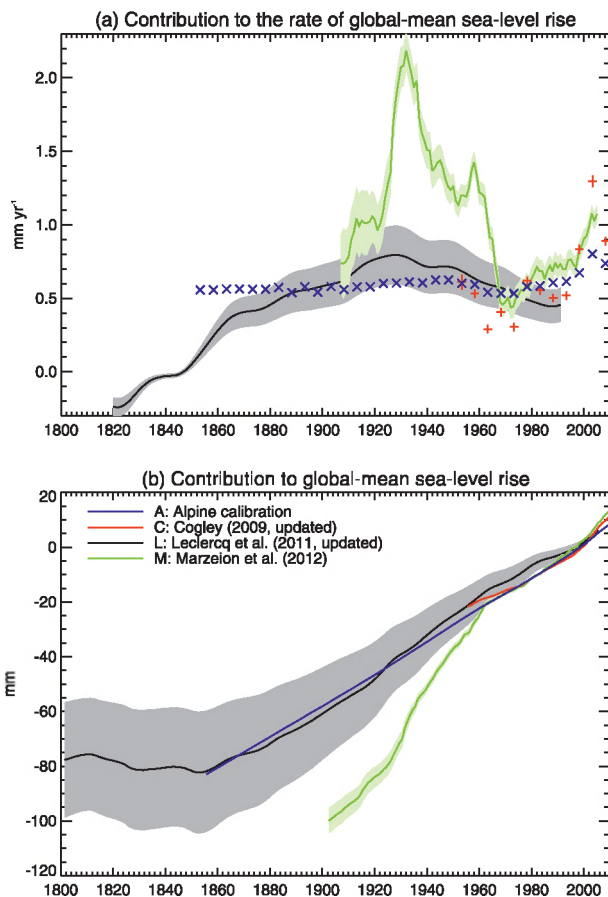


FIG. 2. Time series of the glacier mass contribution to global-mean sea level change. (a) Sea level equivalent of the rate of change of global glacier mass dM_g/dt . The rate for L was calculated by fitting linear trends in overlapping 30-yr periods to the time series of L in (b), the rate for M is the 10-yr running time mean, and the rate for A and C is the time mean of nonoverlapping 5-yr periods. Uncertainties of ± 1 standard error are shown as vertical bars for C and by shading for L and M; the uncertainty of A has not been quantified. (b) Sea level equivalent of the change in global glacier mass ΔM_g , relative to zero for the time mean of 1986–2005. The time series for A, C, and M are the time integrals of those in (a). Uncertainties for A and C are not shown.

Mass gain is not expected globally because the increase in snowfall required to balance the increased ablation is 20–50% K^{-1} (Oerlemans et al. 1998; Braithwaite et al. 2002), an order of magnitude more than the expected increase of global-mean precipitation with global-mean near-surface air temperature. We compare four reconstructions of glacier mass change (Fig. 2), denoted as “glacier C,” “glacier L,” “glacier A,” and “glacier M.” All glaciers and ice caps in the world are taken into account, including those on Greenland and Antarctica, which are marginal to, distinct from, and much smaller than the ice sheets but nonetheless make a substantial contribution to GMSLR (Hock et al. 2009).

a. Glacier C

The most direct method to estimate glacier mass change is from surveys of surface topography change (Cogley 2009; this is referred to as the “geodetic” method), but these have low temporal resolution. An alternative method is measurement of surface mass balance (SMB) $S = P - R$ (Kaser et al. 2006), where P is mass gain (mainly snowfall) and R is mass loss (mainly liquid runoff arising from melting; sublimation is very small for most glaciers). Some glaciers lose ice by discharge (calving) into the sea or lakes; as a separate contribution to mass balance, this is not well measured, but it is included in the geodetic method. Because data are available from each method for only 300–350 of the world’s $\sim 200\,000$ glaciers, they have to be interpolated, and there are too few measurements for a global estimate before 1950. Glacier C is obtained by polynomial interpolation and summation, with appropriate area weighting, to give the rate of change dM_g/dt of global glacier mass as a function of time in 5-yr periods (Cogley 2009, subsequently updated). Hence the change in global glacier mass $\Delta M_g(t)$ is obtained by time integration.

b. Glacier L

Glacier length measurements are available from earlier times than mass change measurements. Based on about 375 glaciers, including 42 calving glaciers, 13 regional time series of fractional glacier length change beginning in the early nineteenth century were constructed by Leclercq et al. (2011, subsequently updated by inclusion of more records, especially for Alaska and Greenland). The unweighted mean of the regional time series was calculated, and this global-mean fractional length time series was converted to a time series of global glacier mass ΔM_g using scaling relations (Bahr et al. 1997; Oerlemans et al. 2007) and calibration against the dataset of Cogley (2009) for 1950 onward.

There is an uncertainty of about 25% (standard error divided by mean) in the results, coming mainly from the limited data coverage of some regions in the datasets of glacier length and mass change; the results are hardly sensitive to uncertainty in the scaling relations (see Leclercq et al. 2011). Considering sea level change with respect to the present day, the uncertainty accumulates and is therefore larger at earlier times (Fig. 6 of Leclercq et al. 2011). Both because glacier length is an integrator of glacier mass balance and because the measurements of terminus position for a given glacier can be widely separated in time, especially earlier in the record, the temporal resolution of glacier L is limited

and hard to evaluate; the e -folding time scale of glacier length adjustment to volume change is typically decades. Therefore, we obtained dM_g/dt from glacier L by linear regression against time in overlapping 30-yr periods. (This is why glacier L ends in 1990 in Fig. 2a, 15 yr before the end of the dataset.)

c. Glacier A

The earliest measurements of mass balance are from the Alps (in Europe) and are derived by the geodetic method from maps made in the 1850s and onward. To the extent that global climate variability and change produce a common response in glaciers worldwide, the rate of change of mass dM_{Alp}/dt of (European) Alpine glaciers might be a proxy for dM_g/dt . The correlation between dM_g/dt and dM_{Alp}/dt in 5-yr periods since 1960 is 0.62. For glacier A, we use the coefficients from a linear regression to estimate dM_g/dt from dM_{Alp}/dt since 1850. There is obviously an unquantified, probably very large systematic uncertainty in this method, but we regard its results as useful corroboration of glacier L.

Glacier A exhibits little variability until the end of the twentieth century. This is because the estimates of dM_{Alp}/dt are less variable than those of dM_g/dt in the dataset of Cogley (2009) and because most of the Alpine measurements before 1950 are geodetic measurements that span many years and so themselves contain little information about short-period variability.

d. Glacier M

Global coverage of climate information is much more complete than the global observational glacier dataset. This motivates the use of models based on climate input (Zuo and Oerlemans 1997; Gregory and Oerlemans 1998; Raper and Braithwaite 2006; Radić and Hock 2011). Marzeion et al. (2012b) calculated glacier mass change throughout the twentieth century from monthly observed near-surface air temperature and precipitation gridded at 0.5° resolution (Mitchell and Jones 2005; New et al. 2002) for every glacier in the Randolph Glacier Inventory (Arendt et al. 2012). Thus, they obtain a time series of global SMB dM_g/dt , which is integrated in time to obtain $\Delta M_g(t)$.

Their method is a refinement of the SMB balance model of Marzeion et al. (2012a), which was originally developed for the Alps, with a new scheme for spatial interpolation of parameters that substantially reduces the potential bias of the original method. The method does not distinguish calving from SMB, but the data used for calibration include some calving glaciers, permitting evaluation of the inaccuracy that arises from assuming the mass changes of these glaciers to have been explained entirely by SMB. The accuracy of the

TABLE 2. Estimates of global-mean sea level rise from tide gauges and of contributory terms, for the periods indicated in the column headings, from datasets spanning the range of years indicated in the rows, expressed as time-mean rate of rise (mm yr^{-1}). The rate is not a trend from linear regression; it is simply calculated as the change in sea level over the period divided by the number of years in the period. We use this statistic in order to avoid making any assumption about the time profile, which might not be well represented by a constant trend during a period of many decades. The uncertainties shown for the tide gauge rates are standard errors, computed from the published uncertainties of the tide gauge datasets. The letters used to identify the datasets are explained in the text. The RMS column, for the tide gauge datasets, is the root-mean-square deviation of annual-mean values (mm) for 1993 onward from a linear regression of GMSLR against time for this period.

		1901–90	1901–2000	1901–70	1971–2005	RMS
Global-mean sea level rise from tide gauges						
TG C	1880–2009	1.46 ± 0.21	1.53 ± 0.19	1.37 ± 0.27	1.98 ± 0.30	3.1
TG J	1700–2002	1.46 ± 0.16	1.70 ± 0.17	1.63 ± 0.19	$1.89 \pm 0.60^*$	5.6
TG R	1900–2006	1.58 ± 0.17	1.73 ± 0.15	1.64 ± 0.22	2.07 ± 0.23	1.5
TG W	1900–2006	1.50 ± 0.28	1.58 ± 0.26	1.51 ± 0.37	1.89 ± 0.19	0.7
Thermal expansion						
Expansion L	1860–2009	0.29	0.31	0.21	0.62	
Expansion M	1860–2009	0.44	0.47	0.32	0.92	
Expansion H	1860–2009	0.58	0.63	0.42	1.22	
Glaciers						
Glacier A	1850–2009	0.59	0.59	0.59	0.63	
Glacier C	1950–2010	—	—	—	0.66	
Glacier L	1800–2005	0.64	0.63	0.68	0.53	
Glacier M	1902–2009	1.09*	1.05*	1.22*	0.73	
Greenland ice sheet						
Greenland B	1840–2011	0.24	0.21	0.31	0.03	
Greenland F	1901–2011	0.01	0.01	0.02	0.05	
Greenland H	1870–2010	−0.27	−0.25	−0.33	−0.02	
Greenland W	1866–2005	0.00	0.00	0.02	−0.01	
Groundwater depletion						
Groundwater K	1900–2008	0.07	0.09	0.04	0.25	
Groundwater W	1900–2009	0.14	0.17	0.09	0.39	
Reservoir impoundment						
Reservoir C	1900–2008	−0.28	−0.29	−0.20	−0.45	
Reservoir L	1890–2009	−0.19	−0.18	−0.15	−0.21	

* Computed from the part of the period that is covered by the dataset.

method is evaluated from a cross-validation procedure. The uncertainty on the time series for glacier M appears to be much smaller than that of glacier L (Fig. 2). In principle this is because of the better coverage of the world's glaciers by meteorological data than by glacier length measurements. However, there are unquantified uncertainties relating to the accuracy of the meteorological data; precipitation in particular is sparsely measured and spatially variable in mountainous regions. In view of this, the uncertainty may be underestimated, particularly in the first half of the twentieth century, for which fewer meteorological observations exist.

e. Comparison

Glaciers A and L were calibrated to match C since 1950, and the model of M was calibrated using some of the same glacier mass balance records as used in C, so the approximate agreement of time-mean rate in recent decades is not unexpected (Table 2). In the last 15 yr, glacier mass has been lost much more rapidly, according to C and M. The effect is less pronounced in A because the mass

loss has been smaller in the Alps (although it certainly has been notable; Zemp et al. 2006; Dyurgerov 2010) and in L because of the lower temporal resolution and because glacier length changes typically lag mass changes.

In the first half of the twentieth century, L and A are similar, while M indicates much greater mass loss, especially in the 1920s and 1930s. Consequently, L and A yield twentieth-century glacier contributions to GMSLR of ~ 60 mm, but M gives ~ 100 mm (Fig. 2b and Table 2). The difference between L and M, which both use data from glaciers worldwide, has two probable causes.

First, they differ in respect of the upscaling procedure used to obtain a global estimate from the sparse observational dataset. Although they are based on different glacier inventories, the world glacier area in L and M is very similar; the difference comes from sensitivity to their assumptions about how the geographical variation in mass balance for the vast majority of unmeasured glaciers is represented by the small sample of measured glaciers. L depends on the interpolation and area weighting of C, against which it is calibrated. M models

each glacier individually, using an implicit assumption that glacier dynamical relaxation time and the time history of regional climate are characteristics that can be geographically interpolated.

Second, there was a warm period in the Arctic and Greenland in the 1920s and 1930s (Box 2002; Johannessen et al. 2004; Kobashi et al. 2011) at a time when anthropogenic global warming was relatively small (see, e.g., Fig. 9.5 of Hegerl et al. 2007). This promoted glacier mass loss at high latitudes in the Northern Hemisphere (e.g., Oerlemans et al. 2011) at a greater rate than the global mean. Although in L the difference is not striking in general (not shown; L includes 79 glaciers north of 60°N and 24 north of 70°N), it is pronounced in Greenland. Length records included in L indicate a greater rate of glacier retreat in the first than in the second half of the twentieth century in Greenland (Leclercq et al. 2012), while in M the warm conditions in the decades concerned produce strongly negative SMB of Greenland glaciers. However, the magnitude of the resulting contribution to GMSLR is larger in M than in L. This discrepancy could be due to deficiencies in the observational climate data, in the sampling of glacier length changes, or in both.

Regardless of these differences, which require further investigation to resolve, all the time series agree that the glacier contribution to GMSLR was substantial throughout the century. Moreover, in both L and M the rate of glacier mass loss was no greater in the second than in the first half of the century. Given the independence of their data sources and method, this is likely to be a robust conclusion, but it is the opposite of the expectation from global warming (cf., e.g., Zuo and Oerlemans 1997).

Apart from the effect of early-century warming in high northern latitudes, as already discussed, a possible explanation is that, as glacier mass is lost, glacier area is reduced, especially the low-altitude ablation area, opposing the tendency to an increasing rate of mass loss (Leclercq et al. 2010). Evidence of this effect can be seen in A, which shows that dM_{Alp}/dt per unit area for Alpine glaciers, from which it is derived, was fairly constant until the last two decades, despite the warming climate. However, Alpine glaciers have lost large areas at low altitudes since the nineteenth century (their area has halved since 1850; Zemp et al. 2006). If the glaciers today had their extent of the late nineteenth century, dM_{Alp}/dt per unit area would not be the same as it was then but far more negative. [SMB per unit area is also affected, but less strongly, by surface lowering (Paul 2010; Huss et al. 2012).] The model of Slangen and van de Wal (2011), which uses power-law scaling of the volume for evolution of the area, gives results that favor a roughly constant rate of global glacier mass loss during

the twentieth century. Further indirect support for this explanation is that a similar balance of opposing tendencies (more intense mass loss per unit area, accompanied by declining area) leads to a fairly constant rate of glacier mass loss, despite a warming global climate, throughout the twenty-first century in the projections of Radić and Hock (2011, their Fig. 2b) and Marzeion et al. (2012b, their Fig. 22).

4. Greenland ice sheet

Observational estimation of change in the mass M_G of the Greenland ice sheet depends on methods that have become possible only in the last two decades: namely, remotely sensed measurement of surface altitude change from aircraft and satellite (Krabill et al. 2004; Thomas et al. 2006; Zwally et al. 2011), measurement of marginal ice velocity by interferometric synthetic-aperture radar combined with mass budget analysis (Rignot et al. 2008, 2011), and satellite measurement of change in the earth's gravity field (Velicogna et al. 2005; Velicogna 2009; Rignot et al. 2011). For the majority of the twentieth century, we estimate instead the rate of change according to $dM_G/dt = S - D$, where D is ice outflow into the sea and $S = P - R$ is the surface mass balance (as for glaciers). We compare four reconstructions of S (Fig. 3) as described below, denoted as “Greenland F,” “Greenland W,” “Greenland H,” and “Greenland B.”

To obtain dM_G/dt requires consideration of D . Following, for example, Hanna et al. (2005), let us assume that over the reference period of 1961–90 there was no net change in the mass of the ice sheet (noting that this does not exclude local changes in ice thickness), so that $dM_G/dt = 0 \Rightarrow \bar{S} - \bar{D} = 0$, where the overbar denotes a time mean over this period. To support this assumption, we note that $S \simeq D \Rightarrow dM_G/dt \simeq 0$ in 1990 (Rignot et al. 2011) and in the mid-1970s (Rignot et al. 2008). Considering differences $\Delta X \equiv X - \bar{X}$ with respect to the reference period, $dM_G/dt = S - D = \bar{S} + \Delta S - \bar{D} - \Delta D = \Delta S - \Delta D$. Although the observational reconstructions do not show D to be constant during the reference period, we take it to be so as a further assumption, which implies that $\Delta D = 0$ always, and hence $dM_G/dt = \Delta S$, where \bar{S} is calculated for 1961–90. Thus we can treat time series for ΔS as an estimate of dM_G/dt . In section 4d we consider an alternative treatment with time-dependent D .

a. Greenland F

Fettweis et al. (2008, subsequently updated) used annual-mean S for 1970–99 simulated at 25-km resolution by Modèle Atmosphérique Régional (MAR), which is a Greenland regional climate model incorporating

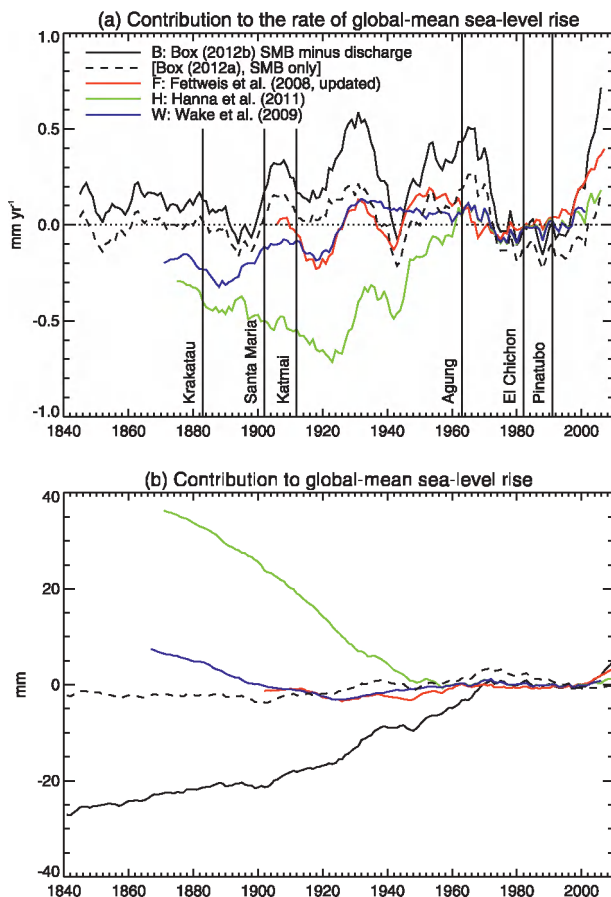


FIG. 3. Time series of the Greenland ice sheet mass contribution to global-mean sea level rise. (a) The 10-yr running time means of the sea level equivalent of the rate of change of mass dM_G/dt of the Greenland ice sheet. F, H, and W are SMB anomalies with respect to the mean of 1961–90. B is the net mass balance, including both SMB and ice discharge. For comparison, SMB from the latter dataset, excluding ice discharge, is shown as a dashed line. The horizontal dotted line indicates zero. The vertical lines indicate the years in which major volcanic eruptions occurred. (b) Sea level equivalent of the change of mass ΔM_G of the Greenland ice sheet, relative to zero for the time mean of 1986–2005. These time series are the time integrals of those in (a).

a surface energy-balance model, with input from the 40-yr European Centre for Medium-Range Weather Forecasts (ECMWF) Re-Analysis (ERA-40; Uppala et al. 2005). They calculated a multiple linear regression of simulated S against observed near-surface air temperature and precipitation data from the Climatic Research Unit (CRU) gridded dataset (Mitchell and Jones 2005; they obtain similar results from other datasets). They selected regions of the ice sheet that gave the best correlation with S for the whole ice sheet; these were the west coast for temperature and the summit for precipitation. They used the regression relationships for these regions to estimate S for 1900–2009 from the CRU dataset (version TS3.10).

b. Greenland W

Wake et al. (2009) computed annual-mean S for 1866–2005 at 5-km resolution using a positive-degree-day model (Janssens and Huybrechts 2000). A reference climate, assumed to be representative of 1961–90 conditions, was perturbed with temperature and precipitation anomalies. For 1958–2002 the anomalies were taken from ERA-40 meteorological reanalyses; after 2002 they were from operational analyses by the ECMWF; and before 1958 they were from correlations between the output of the polar version of the fifth-generation Pennsylvania State University–National Center for Atmospheric Research Mesoscale Model (Polar MM5), which is a Greenland regional climate model, and data from coastal meteorological stations and ice cores (Box et al. 2006, 2009).

c. Greenland H

Hanna et al. (2011) used the same positive-degree-day model and resolution as W for 1870–2010, with climate input from the Twentieth-Century Reanalysis project (Compo et al. 2011) before 1958 and ERA-40 and ECMWF operational analyses thereafter. They made an adjustment to the geographical patterns of precipitation by calibration against the dataset of Bales et al. (2009), which is derived from shallow ice-core data and records of coastal meteorological stations.

d. Greenland B

Box et al. (2013) and Box (2013) used a combination of two Greenland regional climate models, Polar MM5 at 24-km resolution and the Regional Atmospheric Climate Model version 2 (RACMO2) at 11-km resolution, both resampled to 5 km, to simulate the surface climate of the Greenland ice sheet for 1958–2008 with ERA-40 and ECMWF operational analyses as input. They derived empirical relationships between simulated near-surface air temperatures and measurements in order to correct biases in the simulation and to reconstruct temperatures for earlier years. Similarly, they obtained relationships between simulated accumulation and shallow ice-core records (Burgess et al. 2010, supplemented by 25 more records). Thus, they reconstructed accumulation and near-surface air temperature back to 1840, when continuous records of the latter begin, and from these they computed annual-mean S using a positive-degree-day model with coefficients obtained by calibration against in situ observations from 1991 to 2010 of SMB on a transect across the western margin of the ice sheet at 67°N (Van de Wal et al. 2005).

Box and Colgan (2013) took further steps to estimate dM_G/dt . For 1958–2009, they found an empirical

quadratic relationship between the runoff R simulated by Polar MM5 and the solid ice discharge D estimated from ice outflow velocities and ice thickness (Rignot et al. 2008, 2011). During these recent years, D has increased because of the acceleration of many outlet glaciers, probably associated with rise in coastal water temperature (Holland et al. 2008; Hanna et al. 2009; Straneo et al. 2010). Box and Colgan used this relationship to estimate D at earlier times, depending on the idea that climate variability affects runoff and discharge in a correlated way. While this is possible, it has alternatively been argued that runoff could be a negative feedback on coastal water temperature and ice discharge (Murray et al. 2010). After calculating a time series of $dM_G/dt = S - D$, Box and Colgan made a linear adjustment to it by comparison with data from the Gravity Recovery and Climate Experiment (Wahr et al. 2006).

e. Comparison

Greenland F, H, and W all have a similar form for ΔS during 1961–90, as well as zero time mean by construction. The SMB component of B (dotted black line in Fig. 3) has a different time profile and B (including D : solid black line in Fig. 3) has $dM_G/dt = 0.14 \text{ mm yr}^{-1}$ during this period; it is not zero, which is an assumption made by the SMB-only method described above. B increases more rapidly than the other time series after 1990 because of the accelerated outflow D , which is not included in the others.

Throughout the twentieth century, B is almost always positive, with particularly large contributions to sea level during the warm period of the 1920s and 1930s in the Arctic and Greenland, which may have been connected with the North Atlantic Oscillation (Chylek et al. 2004). During this period, B has both large runoff and increased ice discharge. The latter is consistent with evidence showing retreat of many Greenland outlet glaciers (Bjørk et al. 2012), and underlines the influence of D ; although we assumed above that D was constant, it is quite possible that during the twentieth century there could have been substantial fluctuations in D for which we have little observational information. In contrast to B, H almost always gives a negative contribution to GMSLR before 1960 and particularly so in the 1920s; in this reconstruction, SMB in the warm period is dominated by a strong increase in accumulation. Since then, accumulation in H has been decreasing, while it has been increasing in B. F and W are intermediate and markedly different from H before 1960.

All the reconstruction methods depend on ERA-40 and records from coastal meteorological stations, which are the sole or main source of instrumental data for most of the twentieth century and are used in the reanalyses.

Instrumental estimates of precipitation over the ice sheet are particularly limited and subject to uncertainty, which motivates the efforts made to incorporate information from ice cores in B, H, and W. Despite their common inputs, the reconstructions differ substantially, because of their different assumptions and methods. The spread indicates the systematic uncertainty in the estimate of the Greenland ice sheet contribution.

5. Groundwater depletion and reservoir impoundment

Groundwater extraction for agriculture and other uses tends to cause groundwater depletion (i.e., a reduction in the volume of water stored in the subsurface), although the magnitude of depletion arising from extraction is tempered by compensating changes in other water fluxes, such as groundwater recharge and discharge. Groundwater depletion transfers water from the land to the ocean and thus makes a positive contribution to GMSLR. This contribution has been estimated by Konikow (2011) (groundwater K) and Wada et al. (2012) (groundwater W, which is a revised version of Wada et al. 2010). Konikow collected reported volume-based estimates from regional groundwater depletion studies and extrapolated them to make a global estimate of groundwater depletion by assuming the ratio of extraction to depletion to be everywhere the same as evaluated in the United States. Wada et al. (2012) estimated the groundwater depletion flux as the difference between reported spatially downscaled country-based extraction rates and groundwater recharge calculated with a global hydrological model (Van Beek et al. 2011), including both natural recharge and recharge from irrigation. In both time series, the rate increases with time. The contribution accumulated during the twentieth century is 9 mm in K and 17 mm in W (Fig. 4 and Table 2). Each of these time series has an uncertainty estimate, but their ranges of uncertainty overlap only slightly.

Reservoir impoundment is of the opposite sign in its sea level contribution. The volume of water accumulated in reservoirs up to 2010 is about 23 mm sea level equivalent (Chao et al. 2008; Lettenmaier and Milly 2009), neglecting silting up and requiring an assumption, which is a source of uncertainty, about how full the reservoirs are on the time mean. An additional negative contribution to GMSLR is caused by seepage from reservoirs into the surrounding land in arid regions; this amounts to 7 mm according to Chao et al. (2008), but information is scarce about this effect and its size is very uncertain.

Silt that is trapped behind the dam reduces the storage capacity of the reservoir (e.g., Sahagian 2000). Chao

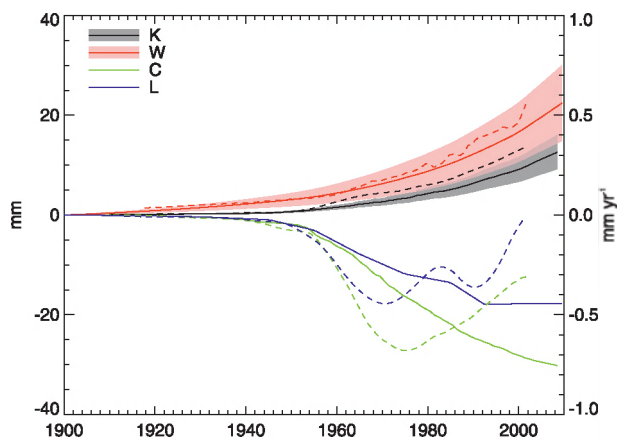


FIG. 4. Time series of contributions to global-mean sea level rise resulting from water resource engineering. Time series K and W are estimates of groundwater depletion, and C and L are estimates of reservoir impoundment. Solid lines and left-hand axis: contributions to global-mean sea level relative to zero in 1900, with uncertainty ranges shown for the two estimates of groundwater depletion. Dashed lines and right-hand axis: contributions to the rate of change of global-mean sea level rise, calculated as a trend in overlapping 20-yr periods, except for W, for which annual rates are shown.

et al. (2008) argue that this is neutral for GMSLR, because silt trapped by dams reduces water storage on land, whereas silt discharged into the ocean raises sea level. An order-of-magnitude calculation casts doubt on this argument. River loads and deposited sediment in the ocean indicate that global solid discharge by rivers is $10\text{--}20 \text{ Gt yr}^{-1}$ (Syvitski et al. 2003; Wilkinson and McElroy 2007; Syvitski and Kettner 2012), or $\sim 5\text{--}10 \text{ km}^3 \text{ yr}^{-1}$ assuming a density of 2000 kg m^{-3} . One estimate of the volume of silt accumulated in reservoirs up to 2010 is about 4 mm sea level equivalent (Lettenmaier and Milly 2009) or $\sim 1400 \text{ km}^3$. This accumulation has taken place over a few decades in those rivers that have been dammed, but it amounts to more than 100 times the global annual solid discharge from all rivers, dammed or not. This comparison suggests that most of the silt trapped by dams would not have reached the ocean; instead, it would have been deposited in alluvial fans and on floodplains. Hence, we argue that silting up has reduced the negative GMSLR contribution of reservoirs. Indeed, silting up of existing reservoirs may already be—or in coming decades may become—a larger effect on impoundment than construction of new capacity (Lettenmaier and Milly 2009; Schleiss et al. 2010), leading to a net positive contribution to the rate of GMSLR from reservoirs.

In view of these uncertainties, as two alternatives we consider the time series of Chao et al. (2008) (reservoir C), which includes seepage but not silting up, and that of

Lettenmaier and Milly (2009) (reservoir L), which includes silting up at 1% of volume per year but not seepage. The former gives -29 mm of GMSLR during the twentieth century; the latter gives -18 mm (Fig. 4 and Table 2).

The net contribution to GMSLR during the twentieth century from groundwater depletion and reservoir impoundment, which can collectively be regarded as contributions from water resource engineering, lies between zero (with groundwater W and reservoir L) and -0.2 mm yr^{-1} (with groundwater K and reservoir C). With the former combination, the net rate would be slightly negative until the 1990s and thereafter a growing net positive contribution, because of accelerating groundwater extraction and decreasing reservoir impoundment. In section 7 we consider all the combinations.

6. Global-mean sea level rise from tide gauge records

a. Comparison and consistency of analyses

We consider four observational time series of GMSLR, all obtained by analysis of the worldwide dataset of tide gauge (TG) records collated by the Permanent Service for Mean Sea Level (<http://www.psmsl.org>). The four time series differ (Fig. 5a) because of the different methods of analysis and selection of records, but they all give a time-mean rate of GMSLR during the twentieth century in the range of $1.5\text{--}1.7 \text{ mm yr}^{-1}$ (Table 2).

Tide gauges measure “relative sea level,” the height of the sea surface with respect to the adjacent land. Hence, for estimates of GMSLR due to change in ocean volume, tide gauge records are corrected for land movement and changes in the gravitational field due to glacial isostatic adjustment (GIA; e.g., Tamisiea and Mitrovica 2011), which is a process with multimillennial time scales causing uplift of regions that were occupied during the last glacial period by ice sheets that have vanished, or by thicker ice sheets than at present, and subsidence of the adjacent regions and of the ocean floor. The corrections to be applied are obtained from GIA models, whose results can locally have large systematic uncertainties, due to assumptions about solid-earth dynamics and the space and time dependence of past changes in ice sheets. These uncertainties tend to cancel out when averaged over many tide gauges because GIA does not change the volume of the global ocean or the solid earth, but the cancellation is not perfect, because the tide gauge network is sparse. Therefore, inaccurate GIA correction could cause a bias in the rate of GMSLR estimated from the tide gauges. By comparing results using various GIA models, Church et al. (2004) and Ray and Douglas (2011) found the

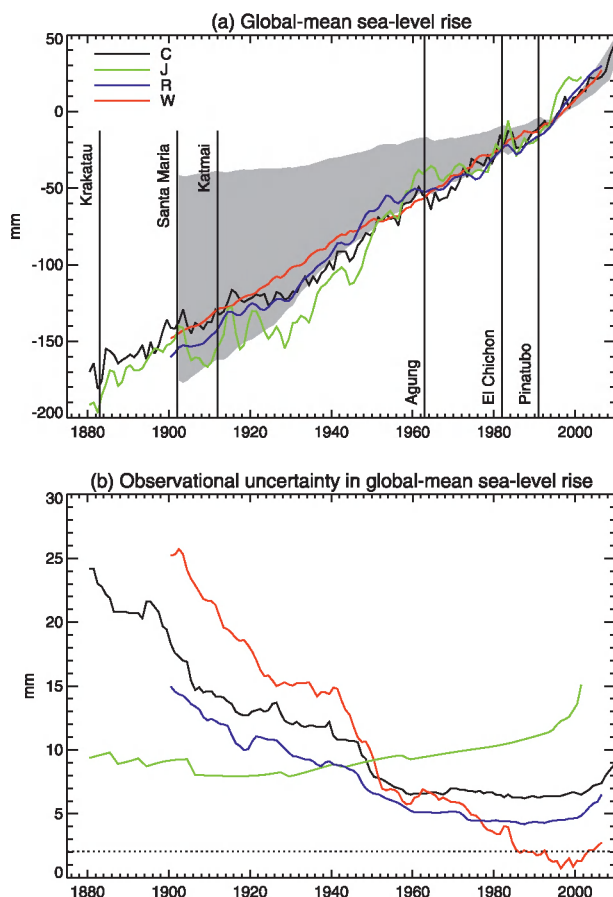


FIG. 5. (a) Comparison of time series of annual-mean global-mean sea level rise from four analyses of tide gauge data (lines) with the range of the 144 synthetic time series (gray shading; see section 7a). Each of the synthetic time series is the sum of a different combination of thermal expansion, glacier, Greenland ice sheet, groundwater, and reservoir time series. All the time series are adjusted to have zero time mean during 1986–2005. The vertical lines indicate the years of major volcanic eruptions. (b) Time series of the uncertainties (standard errors) in annual values from the four tide gauge analyses. The horizontal dotted line is an estimate of interannual variability of global-mean sea level from the altimeter dataset of Nerem et al. (2010).

consequent systematic uncertainty in the rate of GMSLR to be about $\pm 0.1 \text{ mm yr}^{-1}$. Although we cannot formally quantify it, we consider that this uncertainty is adequately reflected by the spread of tide gauge time series that we use, since they employed different GIA models.

Jevrejeva et al. (2008) (time series TG J) use the “virtual station” method of Jevrejeva et al. (2006), which makes an optimal estimate of GMSLR by first averaging the tide gauge records within large regions using weights that attempt to compensate for the inhomogeneous geographical distribution of tide gauges, and then averaging the regions together. Church and White (2011) (time series TG C), Ray and Douglas

(2011) (time series TG R), and Wenzel and Schr  ter (2010) (time series TG W) all combine information about the geographical patterns of variability from the satellite altimeter dataset with information about temporal variations on multidecadal time series from the tide gauge network. The advantage of using the satellite record is its near-global coverage with high spatial resolution, whereas the tide gauge network is sparse and coastal. The weakness is that the spatial patterns of variability exhibited in the last 20 yr might not be representative of longer time scales.

To combine the tide gauge and satellite datasets, Wenzel and Schr  ter (2010) train a neural network to relate them, while Church and White (2011) and Ray and Douglas (2011) use empirical orthogonal functions of the satellite data with principal components derived from the tide gauge records. Church and White analyze changes in sea level over time, enabling them to use many tide gauges, some with short records, without needing to relate the absolute level of different tide gauges. Ray and Douglas analyze absolute sea level, with the vertical reference datum of each tide gauge being part of their solution; this approach means they use only the fewer long records, but they do not need to integrate in time.

Each of the TG time series has uncertainty estimates for its annual values (Fig. 5b). We have compared the annual differences between each pair of TG time series (not shown) with a 5%–95% confidence interval for consistency with zero, computed from the combination in quadrature of their time series of uncertainties, meaning that $\sigma(x - y)$, the standard error of the difference between two quantities x and y , is taken to be $\sqrt{\sigma(x)^2 + \sigma(y)^2}$, as is appropriate if the errors in x and y are independent and normally distributed. We judge the two TG time series to be inconsistent if their difference is inconsistent with zero in more than 10% of years. By this criterion, C, R, and W are consistent but J differs from the other three.

b. Acceleration and decadal variability

Wenzel and Schr  ter (2010) and Ray and Douglas (2011) report that there is no significant acceleration of GMSLR in their time series. On the other hand, Jevrejeva et al. (2008) evaluate the acceleration of GMSLR as about 0.01 mm yr^{-2} for 1700–2003, while Church and White (2011) find $0.009 \pm 0.004 \text{ mm yr}^{-2}$ for 1900–2009. Church and White (2006) report an acceleration of $0.013 \pm 0.006 \text{ mm yr}^{-2}$ for 1870–2001 in an earlier version of the dataset of Church and White (2011). In this paper, we do not show results for the earlier version, but we have analyzed it in the same way as the other four tide gauge time series and the results are close to those we obtain for the later version.

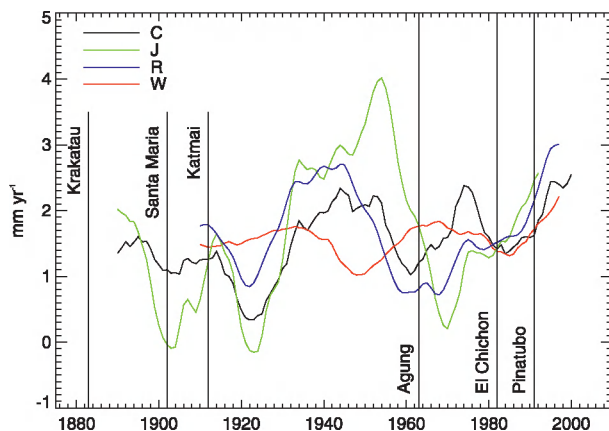


FIG. 6. Comparison of time series of the rate of global-mean sea level rise, from four analyses of tide gauge data, obtained by linear regression against time in overlapping 20-yr periods. Each value of the trend is plotted at the center of the time interval from which it is evaluated. The vertical lines indicate the years of major volcanic eruptions.

To examine further the question of acceleration, we plot the rate of GMSLR, evaluated as the trend from linear regression against time in overlapping 20-yr periods, in each of the four time series (Fig. 6). It is obvious that the time series contain large decadal variability, which would tend to obscure acceleration and other responses to forcing. This variability is not strongly correlated among them. There is a large negative excursion in the rate of GMSLR in C, R, and J around the time of the Agung eruption, but in J its minimum is later (if the same feature) and in W it is absent (in fact opposite). All the time series but W show a marked negative deviation in the early 1920s, when there is no known large volcanic eruption. None of the time series shows a significant reduction in rate due to Pinatubo.

Sea level has large spatial and temporal variability, which is poorly sampled by the tide gauge network; it is very likely that this leads to unrealistically large interannual and decadal variability in the global-mean estimates, depending on the analysis method. The root-mean-square (RMS) residual of annual-mean global-mean sea level about the trend line for linear regression against time during 1993–2008 is shown in the last column of Table 2 for each of the four time series; it is most in J and least in W. The same statistic is 2.1 mm evaluated from the altimeter dataset. W and R have less variability than this; C and J have more. However, except for W in the last three decades, this magnitude of variability is much smaller than the stated observational uncertainties on the annual values (Fig. 5b), implying that the tide gauge datasets do not have sufficient precision to measure annual variations of global-mean sea level.

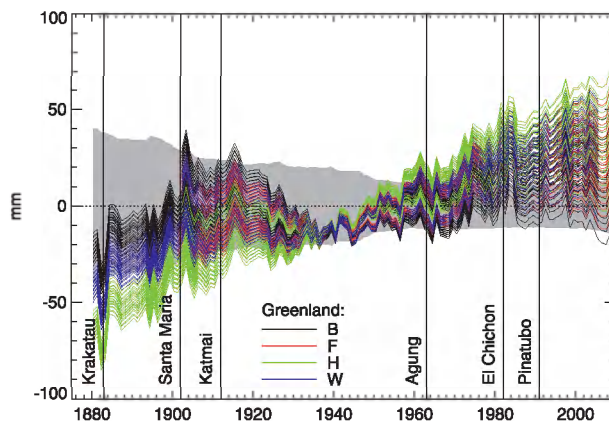


FIG. 7. Time series of differences (TG C minus synthetic) between the observational time series TG C of global-mean sea level rise and the 144 synthetic time series, whose colors indicate which time series each uses for the Greenland ice sheet contribution. The horizontal dotted line indicates zero. The gray shading indicates the 5%–95% confidence interval for consistency with zero. The time series are adjusted to have zero time mean during 1901–90. The vertical lines indicate the years in which major volcanic eruptions occurred.

7. Sea level budget

In this section we consider whether the quantified contributions to GMSLR (sections 2–5) add up to explain the observed GMSLR (section 6). The budget will be incomplete unless we include the contribution from the Antarctic ice sheet. Unfortunately, there are no reliable observational estimates of the trend in the mass or in the mass fluxes of this ice sheet before the satellite era or any model studies for the whole twentieth century with input from meteorological observations. We therefore omit the Antarctic contribution and expect it to contribute a residual to the budget (section 7e).

a. Comparison of synthetic and observed GMSLR

We construct $3 \times 3 \times 4 \times 2 \times 2 = 144$ synthetic time series of GMSLR, with each being the sum of one of the distinct combinations of time series of contributions from thermal expansion (three alternatives), glaciers (three alternatives; glacier C is excluded because it does not span the entire twentieth century), the Greenland ice sheet (four alternatives), groundwater (two alternatives), and reservoirs (two alternatives). We compare the range of the synthetic time series with the TG time series (Fig. 5a), after adjusting all of them to have zero time mean during 1986–2005. The greatest twentieth-century GMSLR in the synthetic time series is about 180 mm, at the upper limit of the observations, and the least is about 40 mm. It is thus evident that the GMSLR in the synthetic time series is generally smaller than observed.

Figure 7 shows the difference between time series TG C, as an example, and each of the 144 synthetic time series individually. Qualitatively similar results are found for the other TG time series (not shown). The time series of differences are all adjusted to have zero time mean during 1901–90 (i.e., the twentieth century, except for its last decade), making them negative at the start of the century and positive at the end because the synthetic time series have less GMSLR than TG C. Up to about 1950 the size of the discrepancy is most strongly dependent on which Greenland estimate is used, with Greenland B giving the smallest residual and Greenland H giving the largest. After this date, the Greenland time series are more similar (Fig. 3a).

We can make a more formal assessment of consistency between a TG time series and a synthetic time series by comparing their difference with zero, allowing for uncertainties. We would expect the synthetic time series to have less variability than GMSLR in the real world on time scales of a few years because the thermal expansion contribution, having been obtained from the ensemble mean of AOGCMs, lacks unforced variability. We therefore attribute a constant standard error of 2.1 mm to the synthetic time series, which is the magnitude of interannual variability that we estimated from the altimeter record. We combine this in quadrature with the time-dependent standard error of annual values for the TG time series, which is typically much larger (Fig. 5b). From the combined time-dependent standard error we construct a 5%–95% envelope for confidence that the difference is consistent with zero (gray shading in Fig. 7). We would judge that a given synthetic time series gave a satisfactory account of observed GMSLR if it lay within the uncertainty envelope for 90% of the time. Very few of the synthetic time series pass this test.

b. Balancing the budget

An additional contribution having a time series that matches the residual (Fig. 7 for the example of TG C) would close the budget. It appears that this would be a fairly constant positive additional trend (i.e., a straight line in Fig. 7); because of the large variability, we do not consider that any curvature could be robustly quantified. For each of the $4 \times 144 = 576$ combinations of TG and synthetic time series, we quantify the required trend by linear regression of the residual against time for 1901–90 and summarize the results graphically (Fig. 8a). In this section, we do not consider the source of the residual; possibilities are discussed in sections 7c–7e.

The 1990s are omitted from the time means used in Fig. 7 and the calculation of the residual trend because of possible recent increases in the ice sheet contributions due to acceleration of ice outflow from the Antarctic and

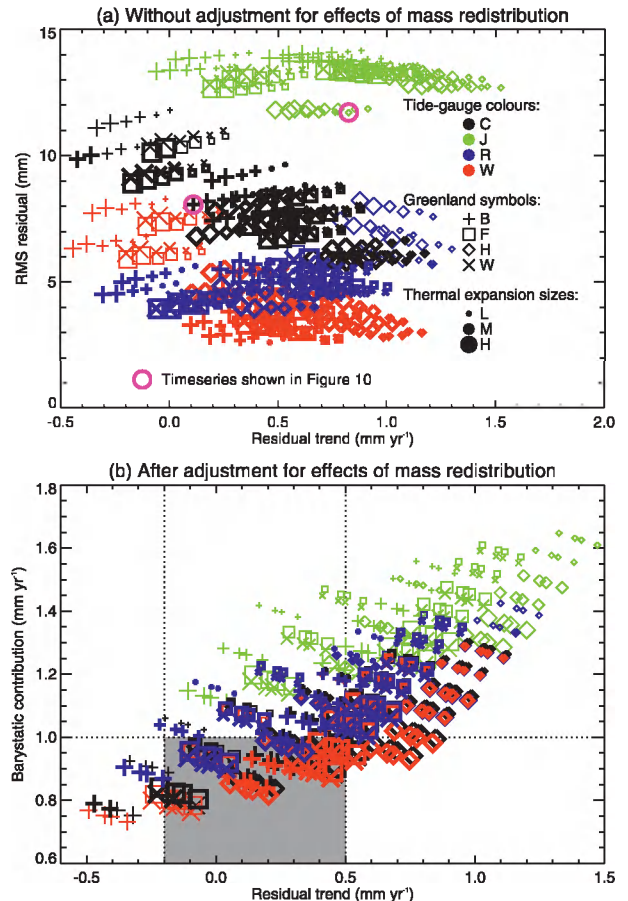


FIG. 8. Analysis of comparison of synthetic and observational time series of global-mean sea level rise. Each symbol indicates the results for one of the possible combinations of TG time series and synthetic time series. The colors indicate which TG time series is used in each case, the symbol size indicates which thermal expansion time series, and the symbol shape indicates which Greenland ice sheet time series. In the key, filled circles are used to indicate the colors and sizes of symbols. The symbols drawn with thick lines indicate cases where the detrended residual is consistent with zero; those drawn with thin lines indicated cases where it is not. For each combination, (a) the residual trend and the RMS of the detrended residual time series and (b) the residual trend and the barystatic contribution (the part from change in the mass of the ocean: i.e., excluding thermal expansion) are shown. In (a) the two combinations whose time series are shown in Fig. 10 are marked. In (b) the TG time series were approximately adjusted for effects of mass redistribution before computing the residual trend; this adjustment decreases the residual trend by $\sim 0.05 \text{ mm yr}^{-1}$. Solutions within the gray shaded area satisfy the constraints described in section 7e. We note that the bounds set by these constraints are not precise.

Greenland ice sheets (Cazenave and Llovel 2010; Church et al. 2011; section 7e). An accelerating contribution could not be represented by a constant residual trend, and these effects are also not included in our contributory time series, except for the empirical estimate of Greenland B (section 4d). The continuous

altimeter record beginning in 1993 (e.g., Nerem et al. 2010) indicates GMSLR at about 3 mm yr^{-1} during 1993–2005, about twice the mean rate for the twentieth century (Table 2). TG reconstructions agree that the rate is higher during the altimeter period than in earlier decades (Church et al. 2011), meaning that the change in rate is not an artifact of the change in observing technology.

The most negative residual trends (plotted as the abscissa in Fig. 8a) are from cases with expansion H (large symbols) and Greenland B (plus symbols), which has a more positive rate of contribution due to the inclusion of ice discharge. The most positive residual trends are from expansion L (small symbols) and Greenland H (diamonds), which has a negative contribution in the early decades of the twentieth century. These differences arise because the residual is smaller if the identified contributions are larger. For the same reason, smaller residual trends tend to be found for glacier M than for glacier L, for groundwater W than for groundwater K, and for reservoir L than for reservoir C. A notable feature of Fig. 8a is that TG J gives larger residual trends than the other three TG time series, even though the time-mean rate of GMSLR during 1901–90 is no larger in TG J than in the others (Table 2). This is because of the particular time profile of TG J, which is discussed below.

We introduce the phrase “retrended synthetic time series” to refer to a synthetic time series plus a constant residual trend line. The reasoning is that

$$\text{TG} - \text{synthetic} = \text{residual} = \text{trend} + \text{deviation}$$

so

$$\begin{aligned} \text{TG} &= \text{synthetic} + \text{trend} + \text{deviation} \\ &= \text{retrended} + \text{deviation}. \end{aligned}$$

That is, a retrended synthetic time series should be similar to the TG time series for which it was constructed; the difference between them is the deviation of the residual from its fitted trend line.

Since

$$\text{TG} - \text{retrended} = \text{deviation} = \text{residual} - \text{trend}$$

we can judge how well the retrended synthetic time series matches the TG time series by examining the residual deviation. To do this, we subtract the fitted trend line from the residual time series, giving a detrended residual time series with zero time mean during 1901–90 (shown for TG C in Fig. 9 as an example), whose RMS we calculate (plotted as the ordinate in Fig. 8a). The size of the RMS depends mostly on the choice of TG time

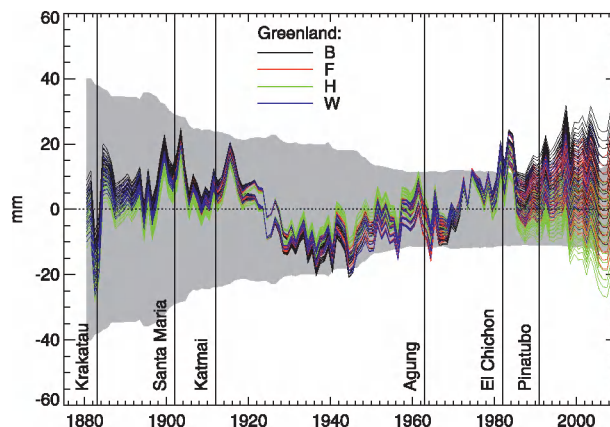


FIG. 9. Time series of the differences shown in Fig. 7 after subtraction of a linear residual trend fitted to 1901–90 for each of the 144 time series separately. The colors indicate which time series for the Greenland ice sheet contribution is used in each case. The horizontal dotted line indicates zero. The gray shading indicates the 5%–95% confidence interval for consistency with zero. The vertical lines indicate the years in which major volcanic eruptions occurred.

series, because of their different magnitude of variability (Table 2); it is smallest for TG W and largest for TG J.

Comparing each detrended residual time series with the uncertainty envelope of its corresponding TG time series (Fig. 9 for the example of TG C), using the same criterion as before, we find that many of the retrended synthetic time series are consistent with TG C, TG R, or TG W (symbols drawn with thick lines in Fig. 8a). They are therefore possible alternative explanations of observed GMSLR. As an example, we show the time series for TG C, expansion H, glacier L, Greenland B, groundwater W, and reservoir L (Fig. 10a). The residual trend in this case is 0.11 mm yr^{-1} . The retrended synthetic time series matches the TG time series quite well. Because the TG time series have a relatively constant rate, consistent solutions tend to require glacier M with Greenland H, so that the large rate of glacier mass loss in the early century is compensated by the gain in Greenland ice sheet mass at the same time.

No synthetic time series is consistent with TG J. TG J has smaller uncertainty than the other time series in the first half of the twentieth century (Fig. 5b) but, if we replace the stated errors of TG J by those of TG C whenever the latter are larger, we still find no consistent solution for TG J. This is because of its much larger interannual and decadal variability, which is reflected in its greater RMS (Table 2 and Fig. 8a). Inspection of the TG time series (Fig. 5a) reveals that TG J departs furthest from a straight line. It has little GMSLR from 1900 to 1930 and then a relatively rapid rise until 1960. These features cannot be well explained by any combination of

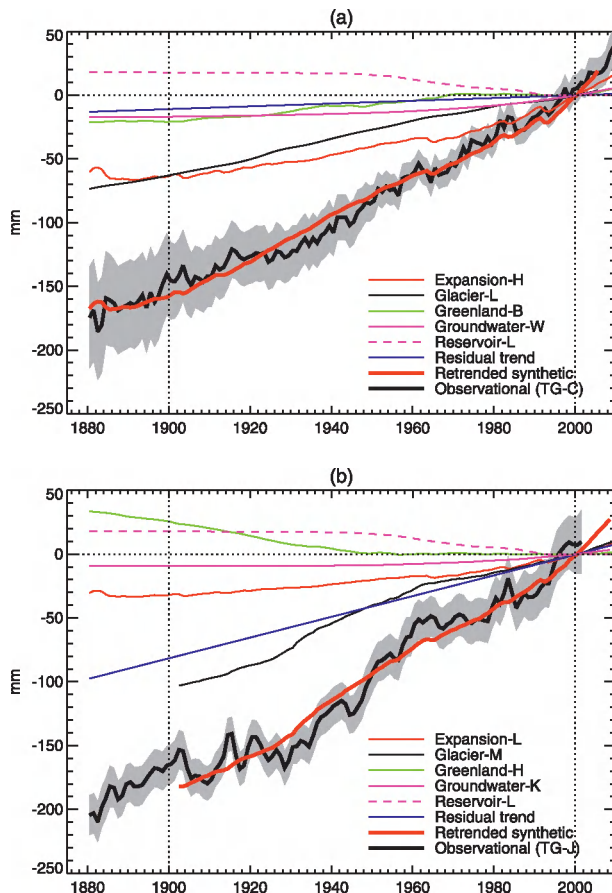


FIG. 10. Two examples comparing an observational and a retrended synthetic time series of global-mean sea level rise (thick lines, with 5%–95% observational uncertainty shaded), also showing the contributions to the latter (thin lines), identified by the time series initials in the key. In each panel, the observational and the retrended synthetic time series have the same time mean during 1901–90, and the latter and its components are all plotted relative to zero in 2000. These examples are two of those shown in Fig. 8a; they do not include the adjustment of 0.05 mm yr^{-1} applied in Fig. 8b. Panel (b) shows the synthetic time series that gives the smallest RMS difference from the observational time series TG J.

our estimates of the contributions. As an example, we show the time series for TG J, expansion L, glacier M, Greenland H, groundwater K, and reservoir L (Fig. 10b). These choices give the smallest obtainable RMS for TG J. The negative contribution from Greenland H helps to account for the small GMSLR trend in the early part of the twentieth century. It is compensated for by a large residual trend of 0.82 mm yr^{-1} . For TG J a constant residual trend cannot close the budget within uncertainties.

c. Coastal oceanographic effects

A possibility to explain the residual is that regional patterns of change in ocean density and circulation

might make the trend in coastal sea level rise exceed the global-mean trend, so that the observational reconstructions overestimate GMSLR. While there are differences associated with climate variability, no such persistent bias is apparent on multidecadal time scales (White et al. 2005; Prandi et al. 2009); on the other hand, model studies of the response to buoyancy forcing indicate that the consequent signal of sea level rise would propagate rapidly around coastlines and radiate more slowly into the ocean far offshore (Hsieh and Bryan 1996; Johnson and Marshall 2002). This is not seen in historical AOGCM simulations (Gregory et al. 2001; White et al. 2005), but these might not adequately resolve coastal ocean dynamics. We have no evidence for such an effect but cannot rule it out.

d. Contemporary changes in the gravity field and the solid earth

Transfer of mass from land to ocean or vice versa changes the geoid (the surface of constant geopotential that would define sea level if the ocean were at rest) because it affects the gravitational field and the earth's rotation, and it causes an elastic deformation of the lithosphere (subsidence in places where the load increases and uplift where it decreases). These responses are rapid, unlike the glacial isostatic adjustment for which tide gauge records are corrected (section 6). Subsidence and gravitational attraction due to an increased mass on land cause relative sea level nearby to rise; in compensation, relative sea level falls elsewhere. Note that this phenomenon is distinct from and locally opposed to the effect on global-mean sea level due to the change of ocean volume. Changes in relative sea level due to these effects could bias the estimates of GMSLR from tide gauge datasets.

Fiedler and Conrad (2010) point out that the water impounded in reservoirs raises relative sea level at nearby tide gauges. They estimate that this effect leads to an overestimate of GMSLR by an amount equal to $\sim 40\%$ of the reservoir contribution to GMSLR. However, it depends strongly on the selection of tide gauges and is estimated to be only 0.035 mm yr^{-1} (2%) of GMSLR during the twentieth century in the tide gauge dataset used by Church and White (2011) and Church et al. (2011).

Changes in mass of ice on land likewise affect relative sea level (Mitrovica et al. 2001; Tamisiea et al. 2003) and could bias GMSLR computed from tide gauge datasets. We compute the effect on the GMSLR estimate of Church and White (2011) using the “fingerprints” on relative sea level of changes in mass of the Antarctic ice sheet (assuming this to be the source of our residual trend), the Greenland ice sheet, and glaciers worldwide

(Mitrovica et al. 2011; Cogley 2009). Mass loss from the Antarctic ice sheet causes relative sea level rise larger than the global mean around the coastlines of all the other continents and therefore gives a positive bias to tide gauge estimates of GMSLR, while mass loss from glaciers and the Greenland ice sheet give a negative bias because they are nearer the majority of tide gauges. The net bias is different for each retrended synthetic time series, because they all have different combinations of land-ice contributions. GMSLR for the twentieth century is overestimated by $0.001 \pm 0.037 \text{ mm yr}^{-1}$ ($0\% \pm 2\%$) for those solutions that are consistent within uncertainties. A more accurate calculation would use the time dependence of the contributions and of the distribution of tide gauges, but we expect that the results would be of a similar size.

If thermal expansion were a purely local effect, it would cause greater sea level rise where the ocean is deeper, because the same fractional expansion, when integrated over the water column, would cause a larger absolute expansion in a thicker layer. This does not happen because ocean dynamics adjusts to compensate for changes in sea surface slope, as can be seen by recalling that the gradient of sea surface dynamic topography is unchanged if the density change is horizontally uniform, regardless of the ocean depth [Lowe and Gregory 2006, Eq. (8)]. Consequently, thermal expansion causes a redistribution of ocean mass toward shallower regions (Landerer et al. 2007b,a; Yin et al. 2010; cf. Bingham and Hughes 2012). This in turn causes changes in the geoid due to gravitational self-attraction of the water, and deformation of the lithosphere due to the greater load on the continental shelves, resulting in relative sea level change at the coast.

We have calculated this effect as an example from the HadGEM1 AOGCM (Johns et al. 2006) under a standard idealized scenario of atmospheric CO_2 increasing at $1\% \text{ yr}^{-1}$, reaching double its initial concentration at year 70. Changes in local ocean density are caused by redistribution of salinity as well as temperature change. In the time mean of years 61–80, GMSLR due to thermal expansion is 95 mm relative to the control state. The distribution of relative sea level change due to self-attraction and loading (Fig. 11) ranges from -4% to $+14\%$ of GMSLR because of thermal expansion, with maxima in the Arctic coastal seas north of Eurasia, because these are the largest regions of shallow ocean in the world and hence have the greatest concentration of mass increase. In general, the effect is positive in the Northern Hemisphere and negative in the Southern Hemisphere, because of the distribution of the continents. Hence, the mean over all coastal grid boxes is positive too, amounting to $+2.6 \text{ mm}$, which would give a 3% overestimate in GMSLR because of thermal

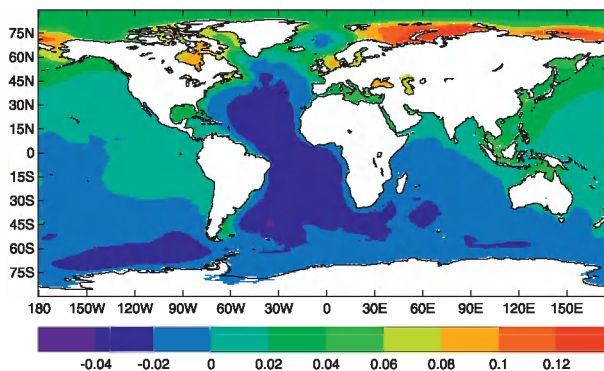


FIG. 11. Effect on relative sea level of the gravitational self-attraction and loading due to the change in ocean density simulated by the HadGEM1 AOGCM for a climate of twice the initial CO_2 concentration. The relative sea level change is shown as a fraction of the global-mean sea level rise due to thermal expansion.

expansion, or about 1% of GMSLR in total (e.g., expansion M accounts for about a third of GMSLR during 1901–2000 in Table 2).

We expect this result to be fairly model independent, because the change in mass distribution depends mostly on ocean bathymetry, rather than on the distribution of density change. If the density change were uniform throughout the volume of the ocean, it is easy to show that the local mass change would be $m = h\rho_0(1 - HA/V)$, where h is GMSLR due to thermal expansion, ρ_0 is a reference density, H is the local ocean depth, A is the surface area of the global ocean, and V is its volume. In regions that are shallow compared with the average ocean depth (i.e., $H \ll V/A$), $m \simeq h\rho_0$, while in the majority of the ocean off the continental shelf, where $H \simeq V/A$, $m \simeq 0$. Landerer et al. (2007a) consider the more general case in which density change is horizontally uniform but depends on depth; their Eq. (3) yields our formula if their $\delta_i \equiv \rho'_i/\rho_0 \rightarrow hA/V$ for all layers i .

This distribution of m shares the main qualitative features of the one predicted from our example of HadGEM1. Its effect on relative sea level (not shown) has a generally similar distribution to m from HadGEM1, but it exaggerates the contrast between shallow and deep areas and the mean over coastal grid boxes is about twice as large. We believe that the HadGEM1 case is more realistic, because we expect warming to be relatively small in the deep ocean, so the simplifying assumption of uniform density change probably overestimates the movement of mass away from deep regions. This bias can be predicted by comparing the predictions of Landerer et al. [2007a, Eq. (3)] for the cases of uniform density change in all levels and in upper levels only.

In summary, it appears that gravitational and solid-earth effects could lead to a small overestimate of

GMSLR by tide gauges. Together they could amount to $3\% \pm 2\%$ of GMSLR, or $\sim 0.05 \text{ mm yr}^{-1}$ (to one significant figure).

e. Constraints on the budget

To allow approximately for the effects of mass redistribution, we reduce the rate of GMSLR from each tide gauge time series by a constant 0.05 mm yr^{-1} (section 7d) and recalculate the residuals from the synthetic time series (section 7b). Thus, we obtain residual trends that are correspondingly reduced (Fig. 8b).

If there is a residual contribution to GMSLR, its source must be one we have not already included, and a likely candidate is the Antarctic ice sheet. Surface melting is negligible in Antarctica, and in the models whose temporal variability is deemed most reliable no significant trend is present in accumulation over recent decades (Monaghan et al. 2006; Lenaerts et al. 2012). As in the case of Greenland (section 4d), satellite observations during the last couple of decades reveal increasing Antarctic ice loss (e.g., Rignot et al. 2011), caused by accelerating ice discharge, which is likely to be a dynamical response to the thinning of ice shelves, especially in the Amundsen Sea. Possibly this could be a consequence of a long-term process (Jenkins et al. 2010), or it might be due to recent incursion of warmer water onto the Antarctic shelf caused by regional wind stress changes (Thoma et al. 2008; Hellmer et al. 2009). At present we do not have any information about the magnitude of decadal variation in Antarctic discharge or SMB earlier in the twentieth century or about its longer-term variability or trends. A constant rate of Antarctic mass loss during 1901–90 is therefore a parsimonious assumption, consistent with the limited information available.

The Antarctic ice sheet could have been losing mass during recent millennia in response to long-term climate change since the Last Glacial Maximum. In an ice sheet model integrated through the last four glacial cycles and from 1500 onward with a constant climate (i.e., excluding recent climate change), Antarctica contributes 0.2 mm yr^{-1} to GMSLR during the twentieth century as a result of ongoing adjustment to previous climate change (Huybrechts et al. 2011). It is thus a possible source of a small positive residual trend, which would be fairly constant during a single century if it relates to the adjustment of the topography of the majority of the ice sheet area where ice flows slowly [see results shown in Fig. 11.3 of Church et al. (2001), from Huybrechts et al. (1998)].

If the twentieth-century residual trend comes from contributions that are fairly constant on a millennial time scale, its magnitude is constrained to within

$0.0\text{--}0.2 \text{ mm yr}^{-1}$ by geological evidence for sea levels during the last 2 ka (Bindoff et al. 2007). A constant rate of GMSLR of about 0.1 mm yr^{-1} until the mid-nineteenth century would lie within the uncertainties of the reconstruction of Kemp et al. (2011) from salt-marsh sediments.

The Antarctic ice sheet could make a long-term contribution outside these limits if there had also been other long-term contributions in previous centuries. There are few model studies of thermal expansion during the last millennium (e.g., Gregory et al. 2006; von Storch et al. 2008), and we should be cautious about long-term trends from these experiments because they may be affected by slow adjustment to volcanic forcing (Gregory 2010). There are no published studies of global glacier mass balance on this time scale. Results from Greenland ice sheet models integrated through previous glacial cycles indicate a small long-term imbalance [$+0.02 \text{ mm yr}^{-1}$ from the results of Huybrechts et al. (2004); -0.02 mm yr^{-1} from Huybrechts et al. (2011)]. New proxy records indicate a reduction circa 1600 in the regional rate of relative sea level rise in West Greenland from $+3 \text{ mm yr}^{-1}$ to $0.0 \pm 0.5 \text{ mm yr}^{-1}$ (Long et al. 2012; Wake et al. 2012). It is likely that this inflexion was mainly caused by changes in the mass balance of the Greenland ice sheet in the sense of increasing mass loss (toward a more positive contribution to GMSLR). Thus, the proxy evidence would favor an explanation in which the Greenland contribution was negligible on the long term and increased to a small positive value before the twentieth century, consistent with Greenland B.

However, there is clearly a great deal of uncertainty in such analyses. Our Greenland time series indicate nineteenth-century contributions to GMSLR of between roughly -0.3 and $+0.2 \text{ mm yr}^{-1}$ (Fig. 3a). Taking this as a broad uncertainty range for the long-term Greenland rate and combining it with the long-term GMSLR uncertainty range of $0.0\text{--}0.2 \text{ mm yr}^{-1}$ constrains the long-term Antarctic contribution—and hence the twentieth-century residual trend—to lie within -0.2 and $+0.5 \text{ mm yr}^{-1}$ (e.g., a long-term trend from Antarctica of $+0.3 \text{ mm yr}^{-1}$ and from Greenland of -0.1 mm yr^{-1} would give long-term GMSLR of $+0.2 \text{ mm yr}^{-1}$).

Excluding thermal expansion from each retrended synthetic time series leaves its barystatic component (i.e., from addition of mass to the ocean, assuming the residual derives from the Antarctic ice sheet). The earth's rotation data (length of day and true polar wander) constrain the time-mean barystatic contribution to a maximum of $\sim 1.0 \text{ mm yr}^{-1}$ [this is a relaxation due to Mitrovica et al. (2006) of the constraint discussed by Munk (2002)]. If we simultaneously apply this constraint, the residual trend constraint, and the

requirement of consistency with GMSLR observations (after reducing them by 0.05 mm yr^{-1} , as mentioned at the start of this section, in order to allow for the effects described in section 7d), there are 86 possible solutions (Fig. 8b); none of them includes expansion L or TG J, but all the other possible contributions appear. This is still the case if we use the tighter residual trend constraint of $0.0\text{--}0.2 \text{ mm yr}^{-1}$, which permits 20 solutions.

8. Discussion and conclusions

The title of this paper refers to the difficulty of accounting for the magnitude of twentieth-century global-mean sea level rise (GMSLR) estimated from the tide gauge records. Previous authors have found observed GMSLR to exceed the sum of the quantified contributions, especially in the early decades of the century, when the influence of anthropogenic climate change was small (Hegerl et al. 2007). Consolidating recent advances in various areas, we show that it is possible to reconstruct the time series of GMSLR, within the uncertainties of the observational estimates, in terms of contributions from thermal expansion, glaciers, the Greenland ice sheet, groundwater extraction, reservoir impoundment, and a constant residual rate. The estimates of these terms come from various methods involving both observations and modeling.

Because ocean observations are lacking for the first half of the twentieth century, we use thermal expansion simulated by AOGCMs. Our central estimate of this contribution is somewhat larger than previous authors', because we make an adjustment for the long-term effect of volcanic forcing on ocean heat content. After this adjustment, the ensemble-mean simulation of thermal expansion by AOGCMs including both natural and anthropogenic forcing agrees remarkably well with an observational estimate for the last four decades in both the trend and the transient effect of volcanic eruptions. The larger estimate of thermal expansion helps to account for observed GMSLR without the barystatic contribution needing to exceed the limit derived from the earth's rotation data (Mitrovica et al. 2006).

The largest contribution to GMSLR during the twentieth century was from glaciers, and its rate was no greater in the second half than in the first half of the century, despite the climatic warming during the century. We argue that this could be due to two influences. First, the warm period in high northern latitudes early in the century probably stimulated glacier mass loss in those decades; our global glacier reconstructions disagree on the magnitude of this effect. Second, progressive loss of low-altitude glacier area, which is most

prone to ablation, would counteract the tendency to increasing mass loss per unit area.

The twentieth-century contribution from the Greenland ice sheet is more uncertain, especially its rate of ice discharge into the sea. One reconstruction indicates that the ice sheet was losing mass at a time-mean rate equivalent to about 0.2 mm yr^{-1} of GMSLR during the century; another indicates that it was gaining mass equivalent to -0.3 mm yr^{-1} of GMSLR.

A constant residual trend of $0.0\text{--}0.2 \text{ mm yr}^{-1}$ during the twentieth century could be explained as a long-term contribution, which would be consistent with geological and proxy evidence of sea level change on multimillennial time scales. The size of the constant residual rate depends on which estimates are used for the other terms, and many choices yield residuals within this range. If we interpret the residual trend as a long-term Antarctic contribution, an ongoing response to climate change over previous millennia, we may conclude that the budget can be satisfactorily closed, provided that the other contributions were small on the long term. The Antarctic long-term contribution could be outside this range if the Greenland ice sheet made a compensating long-term contribution, although this is harder to reconcile with the limited available evidence. In any case, it is clear that the ice sheet contributions remain the greatest source of uncertainty, on all time scales, regarding both surface mass balance and dynamics, and especially the Antarctic contribution, for which there are no observationally based estimates before the satellite era.

Of the contributions to our budget of GMSLR, only thermal expansion shows a tendency for increasing rate as the magnitude of anthropogenic global climate change increases, and this tendency has been weakened by natural volcanic forcing. Groundwater depletion and reservoir impoundment are direct human interventions rather than under climatic control; the Greenland ice sheet contribution relates more to regional climate variability than to global climate change; and the residual, attributed to the Antarctic ice sheet, has no significant time dependence. The implication of our closure of the budget is that a relationship between global climate change and the rate of GMSLR is weak or absent in the twentieth century. The lack of a strong relationship is consistent with the evidence from the tide gauge datasets, whose authors find acceleration of GMSLR during the twentieth century to be either insignificant or small. It also calls into question the basis of the semiempirical methods for projecting GMSLR, which depend on calibrating a relationship between global climate change or radiative forcing and the rate of GMSLR from observational data

(Rahmstorf 2007; Vermeer and Rahmstorf 2009; Jevrejeva et al. 2010).

The relatively constant rate of twentieth-century GMSLR requires an explanation for the apparent onset of GMSLR during the nineteenth or early twentieth century (e.g., Jevrejeva et al. 2008; Gehrels and Woodworth 2013), before substantial anthropogenic climate change had occurred. We think it is most likely that, in the latter half of the nineteenth century, sea level was recovering from radiative forcing because of large volcanic eruptions and reduced solar irradiance earlier in that century (Crowley 2000; Gregory et al. 2006). If this was a global climate phenomenon, it could explain the nineteenth-century onset of glacier mass loss indicated by glacier length records. In the early twentieth century, the warming in northern high latitudes probably increased the rate of GMSLR because of mass loss by glaciers and/or the Greenland ice sheet. These natural upward fluctuations of sea level happened to lead into the start of pronounced anthropogenic warming, and the relative constancy of the rate for most of the century was partly due to greater negative volcanic forcing since the 1960s. Further studies of the variability in and contributions to GMSLR during previous centuries would be helpful.

In the last two decades, the rate of GMSLR has been larger than the twentieth-century time mean, because of increased rates of thermal expansion, glacier mass loss, and ice discharge from both ice sheets (Church et al. 2011). There may also be increasing contributions to GMSLR from the effects of water resource engineering: groundwater depletion is a positive and increasing term; the contribution from reservoir impoundment was negative in the twentieth century but may now be positive, as existing reservoirs become silted up.

Although we think that progress has been made toward accounting for twentieth-century GMSLR, it is evident that there are still substantial uncertainties in the contributions and in how they relate to global or regional climate change. A complete explanation remains to be achieved. This is an important goal, because it would put us in a better position to judge the reliability of models of the contributions, to attribute past GMSLR to climate forcings (anthropogenic or natural), and thus to increase our confidence in projecting future sea level rise.

Acknowledgments. We are grateful to Manfred Wenzel and Jens Schröter, Richard Ray and Bruce Douglas, Svetlana Jevrejeva and her colleagues, and Ben Chao and his colleagues for kindly making their datasets available. We thank Ian Allison, Christopher Bernhardt, Mark Hemer, Walter Munk, and the anonymous reviewers for their constructive comments on the paper. We acknowledge the modeling groups for making their

AOGCM output available as part of the CMIP3 multi-model dataset and the Program for Climate Model Diagnosis and Intercomparison (PCMDI) for collecting and archiving these data. The research leading to these results has received funding from the European Research Council under the European Community's Seventh Framework Programme (FP7/2007-2013), ERC grant agreement 247220, project "Seachange." This paper is a contribution to the Australian Climate Change Research Program; JAC and NJW were partly funded by the Australian Climate Change Science Program.

REFERENCES

- Andreassen, L. M., H. Elvehøy, B. Kjølmoen, R. V. Engeset, and N. Haakensen, 2005: Glacier mass-balance and length variation in Norway. *Ann. Glaciol.*, **42**, 317–325, doi:10.3189/172756405781812826.
- Arendt, A., and Coauthors, 2012: Randolph Glacier Inventory 1.0: A dataset of global glacier outlines. Global Land Ice Measurements from Space Tech. Rep., 28 pp. [Available online at http://www.glims.org/RGI/RGI_Tech_Report_V1.0.pdf.]
- Bahr, D. B., M. F. Meier, and S. D. Peckham, 1997: The physical basis of glacier volume-area scaling. *J. Geophys. Res.*, **102**, 20 355–20 362.
- Bales, R. C., and Coauthors, 2009: Annual accumulation for Greenland updated using ice core data developed during 2000–2006 and analysis of daily coastal meteorological data. *J. Geophys. Res.*, **114**, D06116, doi:10.1029/2008JD011208.
- Bindoff, N. L., and Coauthors, 2007: Observations: Oceanic climate change and sea level. *Climate Change 2007: The Physical Science Basis*, S. Solomon et al., Eds., Cambridge University Press, 385–432.
- Bingham, R. J., and C. W. Hughes, 2012: Local diagnostics to estimate density-induced sea level variations over topography and along coastlines. *J. Geophys. Res.*, **117**, C01013, doi:10.1029/2011JC007276.
- Bjørk, A. A., and Coauthors, 2012: An aerial view of 80 years of climate-related glacier fluctuations in southeast Greenland. *Nat. Geosci.*, **5**, 427–432, doi:10.1038/NGEO1481.
- Box, J. E., 2002: Survey of Greenland instrumental temperature records: 1873–2001. *Int. J. Climatol.*, **22**, 1829–1847, doi:10.1002/joc.852.
- , 2013: Greenland ice sheet mass balance reconstruction. Part II: Surface mass balance (1840–2010). *J. Climate*, in press.
- , and W. Colgan, 2013: Greenland ice sheet mass balance reconstruction. Part III: Marine ice loss and total mass balance (1840–2010). *J. Climate*, in press.
- , and Coauthors, 2006: Greenland ice sheet surface mass balance variability (1988–2004) from calibrated polar MM5 output. *J. Climate*, **19**, 2783–2800.
- , L. Yang, D. H. Bromwich, and L.-S. Bai, 2009: Greenland ice sheet surface air temperature variability: 1840–2007. *J. Climate*, **22**, 4029–4049.
- , and Coauthors, 2013: Greenland ice sheet mass balance reconstruction. Part I: Net snow accumulation (1600–2009). *J. Climate*, in press.
- Braithwaite, R. J., Y. Zhang, and S. C. B. Raper, 2002: Temperature sensitivity of the mass balance of mountain glaciers and ice caps as a climatological characteristic. *Z. Gletscherkd. Glazialgeol.*, **38**, 35–61.

- Burgess, E. W., R. R. Forster, J. E. Box, E. Mosley-Thompson, D. H. Bromwich, R. C. Bales, and L. C. Smith, 2010: A spatially calibrated model of annual accumulation rate on the Greenland ice sheet (1958–2007). *J. Geophys. Res.*, **115**, F02004, doi:10.1029/2009JF001293.
- Cazenave, A., and W. Llovel, 2010: Contemporary sea level rise. *Annu. Rev. Mar. Sci.*, **2**, 145–173, doi:10.1146/annurev-marine-120308-081105.
- Chao, B. F., Y. H. Wu, and Y. S. Li, 2008: Impact of artificial reservoir water impoundment on global sea level. *Science*, **320**, 212–214, doi:10.1126/science.1154580.
- Chinn, T., S. Winkler, M. Salinger, and N. Haakensen, 2005: Recent glacier advances in Norway and New Zealand: A comparison of their glaciological and meteorological causes. *Geogr. Ann.*, **87A**, 141–157, doi:10.1111/j.0435-3676.2005.00249.x.
- Church, J. A., and N. J. White, 2006: A 20th century acceleration in global sea-level rise. *Geophys. Res. Lett.*, **33**, L01602, doi:10.1029/2005GL024826.
- , and —, 2011: Sea-level rise from the late 19th to the early 21st century. *Surv. Geophys.*, **32**, 585–602, doi:10.1007/s10712-011-9119-1.
- , J. M. Gregory, P. Huybrechts, M. Kuhn, K. Lambeck, M. T. Nhu, D. Qin, and P. L. Woodworth, 2001: Changes in sea level. *Climate Change 2001: The Scientific Basis*, J. T. Houghton et al., Cambridge University Press, 639–693.
- , N. J. White, R. Coleman, K. Lambeck, and J. X. Mitrovica, 2004: Estimates of the regional distribution of sea level rise over the 1950–2000 period. *J. Climate*, **17**, 2609–2625.
- , and Coauthors, 2011: Revisiting the Earth's sea-level and energy budgets from 1961 to 2008. *Geophys. Res. Lett.*, **38**, L18601, doi:10.1029/2011GL048794.
- Chylek, P., J. E. Box, and G. Lesins, 2004: Global warming and the Greenland ice sheet. *Climatic Change*, **63**, 201–224.
- Cogley, J. G., 2009: Geodetic and direct mass-balance measurements: Comparison and joint analysis. *Ann. Glaciol.*, **50**, 96–100.
- Compo, G. P., and Coauthors, 2011: The Twentieth Century Reanalysis project. *Quart. J. Roy. Meteor. Soc.*, **137**, 1–28, doi:10.1002/qj.776.
- Crowley, T. J., 2000: Causes of climate change over the past 1000 years. *Science*, **289**, 270–277.
- Delworth, T. L., V. Ramaswamy, and G. L. Stenchikov, 2005: The impact of aerosols on simulated global ocean temperature and heat content in the 20th century. *Geophys. Res. Lett.*, **32**, L24709, doi:10.1029/2005GL024457.
- Domingues, C. M., J. A. Church, N. J. White, P. J. Gleckler, S. E. Wijffels, P. M. Barker, and J. R. Dunn, 2008: Improved estimates of upper-ocean warming and multi-decadal sea-level rise. *Nature*, **453**, 1090–1093, doi:10.1038/nature07080.
- Dyurgerov, M. B., 2010: Reanalysis of glacier changes: From the IGY to the IPY, 1960–2008. *Mater. Glyatsiologicheskikh Issledovaniy*, **108**, 1–116.
- Fettweis, X., E. Hanna, H. Gallee, P. Huybrechts, and M. Ericum, 2008: Estimation of the Greenland ice sheet surface mass balance for the 20th and 21st centuries. *Cryosphere*, **2**, 117–129.
- Fiedler, J. W., and C. P. Conrad, 2010: Spatial variability of sea level rise due to water impoundment behind dams. *Geophys. Res. Lett.*, **37**, L12603, doi:10.1029/2010GL043462.
- Forster, P., and Coauthors, 2007: Changes in atmospheric constituents and in radiative forcing. *Climate Change 2007: The Physical Science Basis*, S. Solomon et al., Eds., Cambridge University Press, 129–234.
- Gardelle, J., E. Berthier, and Y. Arnaud, 2012: Slight mass gain of Karakoram glaciers in the early twenty-first century. *Nat. Geosci.*, **5**, 322–325, doi:10.1038/ngeo1450.
- Gehrels, W. R., and P. L. Woodworth, 2013: When did modern rates of sea-level rise start? *Global Planet. Change*, **100**, 263–277.
- Gleckler, P. J., K. AchutaRao, J. M. Gregory, B. D. Santer, K. E. Taylor, and T. M. L. Wigley, 2006a: Krakatoa lives: The effect of volcanic eruptions on ocean heat content and thermal expansion. *Geophys. Res. Lett.*, **33**, L17702, doi:10.1029/2006GL026771.
- , T. M. L. Wigley, B. D. Santer, J. M. Gregory, K. AchutaRao, and K. E. Taylor, 2006b: Krakatoa's signature persists in the ocean. *Nature*, **439**, 675, doi:10.1038/439675a.
- Gregory, J. M., 2010: Long-term effect of volcanic forcing on ocean heat content. *Geophys. Res. Lett.*, **37**, L22701, doi:10.1029/2010GL045507.
- , and J. Oerlemans, 1998: Simulated future sea-level rise due to glacier melt based on regionally and seasonally resolved temperature changes. *Nature*, **391**, 474–476.
- , and Coauthors, 2001: Comparison of results from several AOGCMs for global and regional sea-level change 1900–2100. *Climate Dyn.*, **18**, 225–240.
- , J. A. Lowe, and S. F. B. Tett, 2006: Simulated global-mean sea-level changes over the last half-millennium. *J. Climate*, **19**, 4576–4591.
- , and Coauthors, 2013: Climate models without preindustrial volcanic forcing underestimate historical ocean thermal expansion. *Geophys. Res. Lett.*, **40**, 1600–1604, doi:10.1002/grl.50339.
- Hanna, E., P. Huybrechts, I. Janssens, J. Cappelen, K. Steffen, and A. Stephens, 2005: Runoff and mass balance of the Greenland ice sheet: 1958–2003. *J. Geophys. Res.*, **110**, D13108, doi:10.1029/2004JD005641.
- , J. Cappelen, X. Fettweis, P. Huybrechts, A. Luckman, and M. H. Ribergaard, 2009: Hydrologic response of the Greenland ice sheet: The role of oceanographic forcing. *Hydrol. Processes*, **23**, 7–30, doi:10.1002/hyp.7090.
- , and Coauthors, 2011: Greenland ice sheet surface mass balance 1870 to 2010 based on Twentieth Century Reanalysis, and links with global climate forcing. *J. Geophys. Res.*, **116**, D24121, doi:10.1029/2011JD016387.
- Hegerl, G. C., and Coauthors, 2007: Understanding and attributing climate change. *Climate Change 2007: The Physical Science Basis*, S. Solomon et al., Eds., Cambridge University Press, 663–745.
- Hellmer, H. H., F. Kauker, and R. Timmermann, 2009: Weddell Sea anomalies: Excitation, propagation, and possible consequences. *Geophys. Res. Lett.*, **36**, L12605, doi:10.1029/2009GL038407.
- Hewitt, K., 2011: Glacier change, concentration, and elevation effects in the Karakoram Himalaya, upper Indus basin. *Mt. Res. Dev.*, **31**, 188–200.
- Hock, R., M. de Woul, V. Radić, and M. Dyurgerov, 2009: Mountain glaciers and ice caps around Antarctica make a large sea-level rise contribution. *Geophys. Res. Lett.*, **36**, L07501, doi:10.1029/2008GL037020.
- Holland, D. M., R. H. Thomas, B. de Young, M. H. Ribergaard, and B. Lyberth, 2008: Acceleration of Jakobshavn Isbrae triggered by warm subsurface ocean waters. *Nat. Geosci.*, **1**, 659–664, doi:10.1038/ngeo316.
- Hsieh, W. W., and K. Bryan, 1996: Redistribution of sea level rise associated with enhanced greenhouse warming: A simple model study. *Climate Dyn.*, **12**, 535–544.

- Huss, M., R. Hock, A. Bauder, and M. Funk, 2012: Conventional versus reference-surface mass balance. *J. Glaciol.*, **58**, 278–286, doi:10.3189/2012jogG11J216.
- Huybrechts, P., A. Abe-Ouchi, I. Marsiat, F. Pattyn, T. Payne, C. Ritz, and V. Rommelaere, 1998: Report of the Third EISMINT Workshop on Model Intercomparison. European Science Foundation Rep., 140 pp.
- , J. Gregory, I. Janssens, and M. Wild, 2004: Modelling Antarctic and Greenland volume changes during the 20th and 21st centuries forced by GCM time slice integrations. *Global Planet. Change*, **42**, 83–105.
- , H. Goelzer, I. Janssens, E. Driesschaert, T. Fichet, H. Goosse, and M.-F. Loutre, 2011: Response of the Greenland and Antarctic ice sheets to multi-millennial greenhouse warming in the Earth system model of intermediate complexity LOVECLIM. *Surv. Geophys.*, **32**, 397–416, doi:10.1007/s10712-011-9131-5.
- Imhof, P., A. Nesje, and S. U. Nussbaumer, 2011: Climate and glacier fluctuations at Jostedalsbreen and Folgefonna, southwestern Norway and in the western Alps from the ‘Little Ice Age’ until the present: The influence of the North Atlantic Oscillation. *Holocene*, **22**, 235–247, doi:10.1177/0959683611414935.
- Janssens, I., and P. Huybrechts, 2000: The treatment of meltwater retention in mass-balance parameterizations of the Greenland ice sheet. *Ann. Glaciol.*, **31**, 133–140, doi:10.3189/172756400781819941.
- Jenkins, A., P. Dutrieux, S. S. Jacobs, S. D. McPhail, J. R. Perrett, A. T. Webb, and D. White, 2010: Observations beneath Pine Island Glacier in West Antarctica and implications for its retreat. *Nat. Geosci.*, **3**, 468–472, doi:10.1038/NGEO890.
- Jevrejeva, S., A. Grinsted, J. C. Moore, and S. Holgate, 2006: Nonlinear trends and multiyear cycles in sea level records. *J. Geophys. Res.*, **111**, C09012, doi:10.1029/2005JC003229.
- , J. C. Moore, A. Grinsted, and P. L. Woodworth, 2008: Recent global sea level acceleration started over 200 years ago? *Geophys. Res. Lett.*, **35**, L08715, doi:10.1029/2008GL033611.
- , —, and —, 2010: How will sea level respond to changes in natural and anthropogenic forcings by 2100? *Geophys. Res. Lett.*, **37**, L07703, doi:10.1029/2010GL042947.
- Johannessen, O. M., and Coauthors, 2004: Arctic climate change: Observed and modelled temperature and sea-ice variability. *Tellus*, **56A**, 328–341, doi:10.1111/j.1600-0870.2004.00060.x.
- Johns, T. C., and Coauthors, 2006: The new Hadley Centre climate model (HadGEM1): Evaluation of coupled simulations. *J. Climate*, **19**, 1327–1353.
- Johnson, H. L., and D. P. Marshall, 2002: A theory for surface Atlantic response to thermohaline variability. *J. Phys. Oceanogr.*, **32**, 1121–1132.
- Kaser, G., J. G. Cogley, M. B. Dyurgerov, M. F. Meier, and A. Ohmura, 2006: Mass balance of glaciers and ice caps: Consensus estimates for 1961–2004. *Geophys. Res. Lett.*, **33**, L19501, doi:10.1029/2006GL027511.
- Kemp, A. C., B. P. Horton, J. P. Donnelly, M. E. Mann, M. Vermeer, and S. Rahmstorf, 2011: Climate related sea-level variations over the past two millennia. *Proc. Natl. Acad. Sci. USA*, **108**, 11 017–11 022, doi:10.1073/pnas.1015619108.
- Kobashi, T., K. Kawamura, J. P. Severinghaus, J.-M. Barnola, T. Nakaegawa, B. M. Vinther, S. J. Johnsen, and J. E. Box, 2011: High variability of Greenland surface temperature over the past 4000 years estimated from trapped air in an ice core. *Geophys. Res. Lett.*, **38**, L21501, doi:10.1029/2011GL049444.
- Konikow, L. F., 2011: Contribution of global groundwater depletion since 1900 to sea-level rise. *Geophys. Res. Lett.*, **38**, L17401, doi:10.1029/2011GL048604.
- Krabill, W., and Coauthors, 2004: Greenland ice sheet: Increased coastal thinning. *Geophys. Res. Lett.*, **31**, L24402, doi:10.1029/2004GL021533.
- Landerer, F. W., J. H. Jungclauss, and J. Marotzke, 2007a: Ocean bottom pressure changes lead to a decreasing length-of-day in a warming climate. *Geophys. Res. Lett.*, **34**, L06307, doi:10.1029/2006GL029106.
- , —, and —, 2007b: Regional dynamic and steric sea level change in response to the IPCC-A1B scenario. *J. Phys. Oceanogr.*, **37**, 296–312.
- Leclercq, P. W., and J. Oerlemans, 2012: Global and hemispheric temperature reconstruction from glacier length fluctuations. *Climate Dyn.*, **38**, 1065–1079, doi:10.1007/s00382-011-1145-7.
- , R. S. W. van de Wal, and J. Oerlemans, 2010: Comment on “100-year mass changes in the Swiss Alps linked to the Atlantic multidecadal oscillation” by Matthias Huss et al. (2010). *Cryosphere Discuss.*, **4**, 2475–2481, doi:10.5194/tcd-4-2475-2010.
- , J. Oerlemans, and J. G. Cogley, 2011: Estimating the glacier contribution to sea-level rise for the period 1800–2005. *Surv. Geophys.*, **32**, 519–535, doi:10.1007/s10712-011-9121-7.
- , A. Weidick, F. Paul, T. Bolch, M. Citterio, and J. Oerlemans, 2012: Historical glacier length changes in West Greenland. *Cryosphere*, **6**, 1339–1343, doi:10.5194/tc-6-1339-2012.
- Lenaerts, J. T. M., M. R. van den Broeke, W. J. van de Berg, E. van Meijgaard, and P. K. Munneke, 2012: A new, high-resolution surface mass balance map of Antarctica (1979–2009) based on regional atmospheric climate modeling. *Geophys. Res. Lett.*, **39**, L04501, doi:10.1029/2011GL050713.
- Lettenmaier, D. P., and P. C. D. Milly, 2009: Land waters and sea level. *Nat. Geosci.*, **2**, 452–454, doi:10.1038/ngeo567.
- Long, A. J., S. A. Woodroffe, G. A. Milne, C. L. Bryant, M. J. R. Simpson, and L. M. Wake, 2012: Relative sea-level change in Greenland during the last 700 yrs and ice sheet response to the Little Ice Age. *Earth Planet. Sci. Lett.*, **315**, 76–85, doi:10.1016/j.epsl.2011.06.027.
- Lowe, J. A., and J. M. Gregory, 2006: Understanding projections of sea level rise in a Hadley Centre coupled climate model. *J. Geophys. Res.*, **111**, C11014, doi:10.1029/2005JC003421.
- Marzeion, B., M. Hofer, A. H. Jarosch, G. Kaser, and T. Mölg, 2012a: A minimal model for reconstructing interannual mass balance variability of glaciers in the European Alps. *Cryosphere*, **6**, 71–84, doi:10.5194/tc-6-71-2012.
- , A. H. Jarosch, and M. Hofer, 2012b: Past and future sea-level change from the surface mass balance of glaciers. *Cryosphere*, **6**, 1295–1322, doi:10.5194/tc-6-1295-2012.
- Mitchell, T. D., and P. D. Jones, 2005: An improved method of constructing a database of monthly climate observations and associated high-resolution grids. *Int. J. Climatol.*, **25**, 693–712, doi:10.1002/joc.1181.
- Mitrovica, J. X., M. E. Tamisiea, J. L. Davis, and G. A. Milne, 2001: Recent mass balance of polar ice sheets inferred from patterns of global sea-level change. *Nature*, **409**, 1026–1029, doi:10.1038/35059054.
- , J. Wahr, I. Matsuyama, A. Paulson, and M. E. Tamisiea, 2006: Reanalysis of ancient eclipse, astronomic and geodetic data: A possible route to resolving the enigma of global sea-level rise. *Earth Planet. Sci. Lett.*, **243**, 390–399, doi:10.1016/j.epsl.2005.12.029.

- , N. Gomez, E. Morrow, C. Hay, K. Latychev, and M. E. Tamisiea, 2011: On the robustness of predictions of sea level fingerprints. *Geophys. J. Int.*, **187**, 729–742, doi:10.1111/j.1365-246X.2011.05090.x.
- Monaghan, A. J., and Coauthors, 2006: Insignificant change in Antarctic snowfall since the International Geophysical Year. *Science*, **313**, 827–831, doi:10.1126/science.1128243.
- Moore, J. C., S. Jevrejeva, and A. Grinsted, 2011: The historical global sea-level budget. *Ann. Glaciol.*, **52**, 8–14.
- Munk, W., 2002: Twentieth century sea level: An enigma. *Proc. Natl. Acad. Sci. USA*, **99**, 6550–6555.
- , 2003: Ocean freshening, sea level rising. *Science*, **300**, 2041–2043.
- Murray, T., and Coauthors, 2010: Ocean regulation hypothesis for glacier dynamics in southeast Greenland and implications for ice sheet mass changes. *J. Geophys. Res.*, **115**, F03026, doi:10.1029/2009JF001522.
- Nerem, R. S., D. P. Chambers, C. Choe, and G. T. Mitchum, 2010: Estimating mean sea level change from the TOPEX and Jason altimeter missions. *Mar. Geod.*, **33**, 435–446, doi:10.1080/01490419.2010.491031.
- New, M., D. Lister, M. Hulme, and I. Makin, 2002: A high-resolution data set of surface climate over global land areas. *Climate Res.*, **21**, 1–25.
- Oerlemans, J., 2005: Extracting a climate signal from 169 glacier records. *Science*, **308**, 675–677, doi:10.1126/science.1107046.
- , and Coauthors, 1998: Modelling the response of glaciers to climate warming. *Climate Dyn.*, **14**, 267–274.
- , M. Dyurgerov, and R. S. W. van de Wal, 2007: Reconstructing the glacier contribution to sea-level rise back to 1850. *Cryosphere*, **1**, 59–65.
- , J. Jania, and L. Kolondra, 2011: Application of a minimal glacier model to Hansbreen, Svalbard. *Cryosphere*, **5**, 1–11, doi:10.5194/tc-5-1-2011.
- Paul, F., 2010: The influence of changes in glacier extent and surface elevation on modeled mass balance. *Cryosphere*, **4**, 569–581, doi:10.5194/tc-4-569-2010.
- Prandi, P., A. Cazenave, and M. Becker, 2009: Is coastal mean sea level rising faster than the global mean? A comparison between tide gauges and satellite altimetry over 1993–2007. *Geophys. Res. Lett.*, **36**, L05602, doi:10.1029/2008GL036564.
- Radić, V., and R. Hock, 2011: Regionally differentiated contribution of mountain glaciers and ice caps to future sea-level rise. *Nat. Geosci.*, **4**, 91–94, doi:10.1038/ngeo1052.
- Rahmstorf, S., 2007: A semi-empirical approach to projecting future sea-level rise. *Science*, **315**, 368–370, doi:10.1126/science.1135456.
- Raper, S. C. B., and R. J. Braithwaite, 2006: Low sea level rise projections from mountain glaciers and icecaps under global warming. *Nature*, **439**, 311–313, doi:10.1038/nature04448.
- Ray, R. D., and B. C. Douglas, 2011: Experiments in reconstructing twentieth-century sea levels. *Prog. Oceanogr.*, **91**, 496–515, doi:10.1016/j.pocean.2011.07.021.
- Rignot, E., J. E. Box, E. Burgess, and E. Hanna, 2008: Mass balance of the Greenland ice sheet from 1958 to 2007. *Geophys. Res. Lett.*, **35**, L20502, doi:10.1029/2008GL035417.
- , I. Velicogna, M. R. van den Broeke, A. Monaghan, and J. T. M. Lenaerts, 2011: Acceleration of the contribution of the Greenland and Antarctic ice sheets to sea level rise. *Geophys. Res. Lett.*, **38**, L05503, doi:10.1029/2011GL046583.
- Sahagian, D., 2000: Global physical effects of anthropogenic hydrological alterations: Sea level and water redistribution. *Global Planet. Change*, **25**, 39–48, doi:10.1016/S0921-8181(00)00020-5.
- Schleiss, A., G. De Cesare, and J. J. Althaus, 2010: Verlandung der Stauseen gefährdet die nachhaltige Nutzung der Wasserkraft. *Wasser Energ. Luft*, **102**, 31–40.
- Slangen, A. B. A., and R. S. W. van de Wal, 2011: An assessment of uncertainties in using volume-area modelling for computing the twenty-first century glacier contribution to sea-level change. *Cryosphere*, **5**, 673–686, doi:10.5194/tc-5-673-2011.
- Stott, P. A., N. P. Gillett, G. C. Hegerl, D. J. Karoly, D. A. Stone, X. Zhang, and F. Zwiers, 2010: Detection and attribution of climate change: A regional perspective. *Wiley Interdiscip. Rev. Climate Change*, **1**, 192–211.
- Straneo, F., G. S. Hamilton, D. A. Sutherland, L. A. Stearns, F. Davidson, M. O. Hammill, G. B. Stenson, and A. Rosing-Asvid, 2010: Rapid circulation of warm subtropical waters in a major glacial fjord in East Greenland. *Nat. Geosci.*, **3**, 182–186, doi:10.1038/ngeo764.
- Syvitski, J. P. M., and A. Kettner, 2012: Sediment flux and the Anthropocene. *Philos. Trans. Roy. Soc. London*, **369**, 957–975, doi:10.1098/rsta.2010.0329.
- , S. D. Peckham, R. Hilberman, and T. Mulder, 2003: Predicting the terrestrial flux of sediment to the global ocean: A planetary perspective. *Sediment. Geol.*, **162**, 5–24, doi:10.1016/S0037-0738(03)00232-X.
- Tamisiea, M. E., and J. X. Mitrovica, 2011: The moving boundaries of sea level change: Understanding the origins of geographic variability. *Oceanography*, **24**, 24–39, doi:10.5670/oceanog.2011.25.
- , —, and J. L. Davis, 2003: A method for detecting rapid mass flux of small glaciers using local sea level variations. *Earth Planet. Sci. Lett.*, **213**, 477–485.
- Thoma, M., A. Jenkins, D. Holland, and S. Jacobs, 2008: Modelling circumpolar deep water intrusions on the Amundsen Sea continental shelf, Antarctica. *Geophys. Res. Lett.*, **35**, L18602, doi:10.1029/2008GL034939.
- Thomas, R., E. Frederick, W. Krabill, S. Manizade, and C. Martin, 2006: Progressive increase in ice loss from Greenland. *Geophys. Res. Lett.*, **33**, L10503, doi:10.1029/2006GL026075.
- Uppala, S. M., and Coauthors, 2005: The ERA-40 Re-Analysis. *Quart. J. Roy. Meteor. Soc.*, **131**, 2961–3012.
- Van Beek, L. P. H., Y. Wada, and M. F. P. Bierkens, 2011: Global monthly water stress: 1. Water balance and water availability. *Water Resour. Res.*, **47**, W07517, doi:10.1029/2010WR009791.
- Van de Wal, R. S. W., W. Greuell, M. R. van den Broeke, C. H. Reijmer, and J. Oerlemans, 2005: Surface mass-balance observations and automatic weather station data along a transect near Kangerlussuaq, West Greenland. *Ann. Glaciol.*, **42**, 311–316.
- Velicogna, I., 2009: Increasing rates of ice mass loss from the Greenland and Antarctic ice sheets revealed by GRACE. *Geophys. Res. Lett.*, **36**, L19503, doi:10.1029/2009GL040222.
- , J. Wahr, E. Hanna, and P. Huybrechts, 2005: Snow accumulation and ice discharge in Greenland, from GRACE. *Geophys. Res. Lett.*, **32**, L05501, doi:10.1029/2004GL021948.
- Vermeer, M., and S. Rahmstorf, 2009: Global sea level linked to global temperature. *Proc. Natl. Acad. Sci. USA*, **106**, 21 527–21 532, doi:10.1073/pnas.0907765106.
- von Storch, H., E. Zorita, and J. F. González-Rouco, 2008: Relationship between global mean sea-level and global mean temperature in a climate simulation of the past millennium. *Ocean Dyn.*, **58**, 227–236, doi:10.1007/s10236-008-0142-9.

- Wada, Y., L. P. H. van Beek, C. M. van Kempen, J. W. T. M. Reckman, S. Vasak, and M. F. P. Bierkens, 2010: Global depletion of groundwater resources. *Geophys. Res. Lett.*, **37**, L20402, doi:10.1029/2010GL044571.
- , —, F. C. S. Weiland, B. F. Chao, Y.-H. Wu, and M. F. P. Bierkens, 2012: Past and future contribution of global groundwater depletion to sea-level rise. *Geophys. Res. Lett.*, **39**, L09402, doi:10.1029/2012GL051230.
- Wahr, J., S. Swenson, and I. Velicogna, 2006: Accuracy of GRACE mass estimates. *Geophys. Res. Lett.*, **33**, L06401, doi:10.1029/2005GL025305.
- Wake, L. M., P. Huybrechts, J. E. Box, E. Hanna, I. Janssens, and G. A. Milne, 2009: Surface mass-balance changes of the Greenland ice sheet since 1866. *Ann. Glaciol.*, **50**, 178–184.
- , G. A. Milne, A. J. Long, S. A. Woodroffe, M. J. R. Simpson, and P. Huybrechts, 2012: Century-scale relative sea-level changes in West Greenland—A plausibility study to assess contributions from the cryosphere and the ocean. *Earth Planet. Sci. Lett.*, **315**, 86–93, doi:10.1016/j.epsl.2011.09.029.
- Wenzel, M., and J. Schröter, 2010: Reconstruction of regional mean sea level anomalies from tide gauges using neural networks. *J. Geophys. Res.*, **115**, C08013, doi:10.1029/2009JC005630.
- White, N. J., J. A. Church, and J. M. Gregory, 2005: Coastal and global averaged sea level rise for 1950 to 2000. *Geophys. Res. Lett.*, **31**, L01601, doi:10.1029/2004GL021391.
- Wilkinson, B. H., and B. J. McElroy, 2007: The impact of humans on continental erosion and sedimentation. *Geol. Soc. Amer. Bull.*, **119**, 140–156, doi:10.1130/B25899.1.
- Yin, J., S. M. Griffies, and R. J. Stouffer, 2010: Spatial variability of sea level rise in twenty-first century projections. *J. Climate*, **23**, 4585–4607.
- Zemp, M., W. Haeberli, M. Hoelzle, and F. Paul, 2006: Alpine glaciers to disappear within decades? *Geophys. Res. Lett.*, **33**, L13504, doi:10.1029/2006GL026319.
- Zuo, Z., and J. Oerlemans, 1997: Contribution of glacier melt to sea level rise since AD 1865: A regionally differentiated calculation. *Climate Dyn.*, **13**, 835–845.
- Zwally, H. J., and Coauthors, 2011: Greenland ice sheet mass balance: Distribution of increased mass loss with climate warming; 2003–07 versus 1992–2002. *J. Glaciol.*, **57**, 88–102.